Article:
Akarsu, Ö, Di Valentino, E., Vyskočil, J. et al. (2026) Nonlinear matter power spectrum from relativistic N-body simulations: ΛsCDM versus ΛCDM. Physical Review D, 113 (8). 083508. ISSN: 2470-0010

https://doi.org/10.1103/lmt4-hshz

Nonlinear Matter Power Spectrum from relativistic N-body Simulations: Λ_sCDM versus ΛCDM

Özgür Akarsu,[1,*] Eleonora Di Valentino,[2,†] Jiří Vyskočil,[3,4,‡] Ezgi Yılmaz,[5,§] A. Emrah Yükselci,[1,¶] and Alexander Zhuk[3,4,6,**]

[1] *Department of Physics, Istanbul Technical University, Maslak 34469 Istanbul, Türkiye*
[2] *School of Mathematical and Physical Sciences, University of Sheffield, Hounsfield Road, Sheffield S3 7RH, United Kingdom*
[3] *Center for Advanced Systems Understanding, Untermarkt 20, 02826 Görlitz, Germany*
[4] *Helmholtz-Zentrum Dresden-Rossendorf, Bautzner Landstraße 400, 01328 Dresden, Germany*
[5] *Deutsches Zentrum für Astrophysik, Postplatz 1, 02826, Görlitz, Germany*
[6] *Astronomical Observatory, Odesa I.I. Mechnikov National University, Dvoryanskaya Street 2, Odesa 65082, Ukraine*

We present relativistic N-body simulations of a Λ_sCDM—sign-switching cosmological constant (CC)—scenario under general relativity and compare its nonlinear matter power spectrum to ΛCDM at $z = 15, 2, 1, 0$, using best-fit parameters from *Planck*-only and a combined "full" dataset. During the AdS-like CC ($\Lambda_s < 0$) phase, prior to the transition redshift $z_\dagger$, reduced Hubble friction dynamically enhances the growth of perturbations; after the switch, with dS-like CC ($\Lambda_s > 0$), the larger late-time expansion rate partly suppresses, but does not erase, the earlier amplification. Consequently, the ratio $P_{\Lambda_s\mathrm{CDM}}/P_{\Lambda\mathrm{CDM}}$ exhibits a pronounced, redshift-dependent shape feature: a crest peaking at $\sim 20-25\%$ around $k \simeq 1-3\,h\,\mathrm{Mpc}^{-1}$ near the transition, which then migrates to larger physical scales and persists to $z = 0$ as a robust $\sim 15-20\%$ uplift at $k \simeq 0.6-1.0\,h\,\mathrm{Mpc}^{-1}$. These wavenumbers correspond to group or poor-cluster environments and lie within the sensitivity range of weak lensing, galaxy-galaxy lensing, cluster counts, and tSZ power, providing a concrete, falsifiable target that cannot be mimicked by a scale-independent change in σ_8 or S_8. The timing (earlier for *Planck*-only, later for the full dataset) and the amplitude of the crest align with the "cosmic noon" epoch ($z \simeq 1-2$), offering a gravitational prior for the observed peak in the cosmic star-formation rate.

I. INTRODUCTION

The concordance ΛCDM model remains the simplest and most successful framework for describing the evolution of the Universe, providing an excellent fit to early-universe probes such as the Cosmic Microwave Background (CMB) anisotropies [1–3] and Big Bang Nucleosynthesis (BBN). Nevertheless, in recent years a number of persistent *cosmological tensions* have emerged when ΛCDM predictions are confronted with late-time observations [4–8]. The most prominent is the more than 6σ discrepancy between the value of the Hubble constant (H_0) [9–19] inferred from CMB data [1–3] and that measured by the local distance ladder [20–49], but additional anomalies, such as the so-called S_8 tension [50–71] in weak lensing reinforce the case that ΛCDM, while highly successful, may be incomplete. Proposed solutions are commonly grouped into two broad categories, by when they act on the expansion history: *early-time modifications*, which alter the expansion or energy content before recombination (e.g., early dark energy, EDE [14, 72–82]), and *late-time modifications*, which deform the post-recombination expansion while preserving high-redshift successes of the standard cosmology (e.g., interacting dark energy, IDE [83–102]). In this context, recent results from DESI [103, 104] have sharpened the observational picture, showing that extensions such as *dynamical dark energy* (DDE) [105–132] can substantially improve the joint consistency of BAO and supernova data relative to ΛCDM, further motivating systematic explorations of late-time departures from ΛCDM and possible new physics affecting late-universe dynamics.

Among the realizations of the latter category, the Λ_sCDM framework (also known as the *sign-switching cosmological constant* (CC)) [133–136] stands out as one of the most promising and economical extensions of ΛCDM. It posits that around redshift $z_\dagger \sim 2$, the Universe underwent a rapid *mirror* AdS-to-dS (anti-de Sitter to de Sitter) transition in the vacuum energy: the effective cosmological constant Λ_s flipped from negative to positive while preserving its magnitude ("mirror" reflects this invariance), with all other standard components, including baryons, CDM, pre-recombination physics, and the inflationary paradigm, left unaltered. The idea was originally conjectured phenomenologically in Ref. [133], motivated by hints from the graduated dark energy (gDE) model, where a swift yet smooth mirror AdS-to-dS-like transition passage around $z \sim 2$ helps organize late-time discrepancies (e.g., the H_0 and BAO Lyα discrepancies) without disturbing CMB-era physics. Phenomenologically, such transitions can be described with sigmoid-like profiles; for example, $\Lambda_s(z) = \Lambda_{s0}\,\frac{\tanh[\eta\,(z_\dagger - z)]}{\tanh(\eta z_\dagger)}$, where $\eta > 1$ controls the sharpness, $\Lambda_{s0} > 0$ is the present-day value, and $z_\dagger$ denotes the

* akarsuo@itu.edu.tr
† e.divalentino@sheffield.ac.uk
‡ j.vyskocil@hzdr.de
§ ezgi.yilmaz@dzastro.de
¶ yukselcia@itu.edu.tr
** ai.zhuk2@gmail.com

center of the transition [135]. For sufficiently rapid transitions (e.g., $\eta \gtrsim 10$ at $z_\dagger \sim 2$), this approaches a smooth step with $\Lambda_s \approx \Lambda_{s0}$ for $z \lesssim 2$ and $\Lambda_s \approx -\Lambda_{s0}$ for $z \gtrsim 2$, effectively leaving a single parameter, $z_\dagger$ [135, 137]. In the instantaneous limit $\eta \to \infty$, $\Lambda_s(z) \to \Lambda_{s0}\,\mathrm{sgn}(z_\dagger - z)$, which defines the *abrupt* Λ_sCDM model [134–136], an idealized representation of a rapid mirror AdS-to-dS transition that extends ΛCDM by a single additional parameter, $z_\dagger$. This simplest phenomenological realization of Λ_sCDM has been extensively studied under the assumption of GR; see, e.g., Refs. [134–141]. The abrupt limit serves as a controlled proxy for a fast transition, and by construction the limit $z_\dagger \to \infty$ exactly recovers ΛCDM. We refer the reader (without claiming completeness) to the broader literature on Λ_sCDM and cognate scenarios, including theoretical developments, observational constraints, and related frameworks that invoke a negative CC or DE sectors (effective or field-based) admitting negative energy densities at high redshifts, as well as model-agnostic reconstructions pointing in that direction; see Refs. [93, 100, 112, 121, 124, 139–230].

In Λ_sCDM, because the pre-recombination universe remains unaltered, CMB distance anchoring *forces* a compensating late-time shift that *raises* H_0 while *lowering* Ω_{m0}. Consequently, as shown in a series of studies (e.g., [134–139]), raising H_0 to Supernovae and H0 for the Equation of State of Dark Energy (SH0ES) values naturally suppresses the present-day growth rate $f_0 \simeq \Omega_{m0}^{\gamma}$ (while retaining the GR benchmark $\gamma \simeq 0.55$ for the growth index) and the clustering metric $S_8 \equiv \sigma_8 \sqrt{\Omega_{m0}/0.3}$ (even though σ_8 increases slightly), thereby enabling Λ_sCDM to simultaneously address the H_0, S_8, and γ tensions *without* invoking modified gravity. Moreover, the framework remains compatible with BAO Lyα data at $z_{\rm eff} \sim 2.3$, with estimates of the present age of the Universe from the oldest globular clusters, and (with neutrino parameters treated as free [138]) with standard neutrino properties. Notably, a rapid transition near $z_\dagger \approx 1.7$ has been identified as the model's "sweet-spot", where these achievements are realized simultaneously [134–139].

Crucially, the departures of the abrupt Λ_sCDM scenario from ΛCDM are *dynamical* and begin before the transition, namely in the AdS epoch of Λ_s [134]. They arise in the background expansion and, consequently, in the evolution of perturbations, and hence in structure growth. Specifically, for a transition at $z_\dagger \sim 2$ (as suggested by observational analyses [134–137]), observable departures are confined primarily to the $z \lesssim 3$ universe. By $z \sim 3$, the dark energy fraction is only a few percent, $\Omega_\Lambda(z \sim 3) \simeq |\Omega_{\Lambda_s}(z \sim 3)| \sim \mathcal{O}(10^{-2})$, and rapidly becomes negligible, so that for $3 \lesssim z \lesssim z_{\rm eq} \simeq 3400$, both models are effectively Einstein–de Sitter and, for $z > z_{\rm rec} \simeq 1100$, reproduce the standard pre-recombination cosmology. The fundamental difference, relative to ΛCDM, is that in the AdS-like CC era ($z > z_\dagger$), the expansion rate $H(z)$ is *lower*, with the deficit growing toward the transition and most pronounced for $z_\dagger < z \lesssim 3$, whereas after the transition (dS-like CC era, $z < z_\dagger$), $H(z)$ is *higher* while closely tracking the ΛCDM redshift dependence. Taken together, these shifts are expected to have clear and distinct dynamical implications for structure growth.

Accordingly, in the absence of dark energy clustering, subhorizon (pressureless) matter perturbations obey $\ddot{\delta} + 2H\dot{\delta} - 4\pi G \rho_m \delta = 0$ [135, 141]. Hence, owing to the $H(z)$ evolution described above and *relative* to ΛCDM, the Hubble friction term $2H\dot{\delta}$ is increasingly suppressed across the AdS window (toward the transition), leading to progressively enhanced growth. After the transition, although Λ_s is dS-like as in ΛCDM, $H(z)$ is larger and the friction term becomes more pronounced, thereby damping growth more efficiently throughout that era. Consequently, while in both models the growth index attains the Einstein–de Sitter value $\gamma_{\rm EdS} = 6/11$ at recombination, in the post-recombination era ΛCDM has $\gamma(a) > \gamma_{\rm EdS}$, with an excess that increases toward low z. In contrast, in Λ_sCDM it remains *below* $\gamma_{\rm EdS}$ throughout the dS-like CC era, with a deficit that strengthens toward $z_\dagger$. At the transition, it jumps sharply and thereafter *raises* smoothly toward low z, tracking the ΛCDM curve at slightly higher values while remaining close to the GR benchmark $\gamma \simeq 0.55$ overall (see Ref. [141], Fig. 11).

Correspondingly, relative to ΛCDM, Λ_sCDM exhibits a progressively enhanced growth rate $f(a)$ throughout the AdS-like CC era, peaking just before the transition (by $\sim 15\%$ for $z_\dagger \sim 2$; see Ref. [141], Fig. 10). At the switch, $f(a)$ drops slightly below the ΛCDM value; thereafter, in the dS-like CC era, it follows the ΛCDM redshift dependence while remaining lower. This behavior of $f(a)$ in Λ_sCDM renders the model a natural candidate to alleviate the recently identified growth-index (γ) tension in ΛCDM [231]. For context, we briefly outline the mechanism (see Refs. [139, 141] for details). In ΛCDM, adopting the Planck-anchored $\Omega_{m0} = 0.32$ together with the GR benchmark $\gamma \simeq 0.55$ yields $f_0 = \Omega_{m0}^{\gamma} \simeq 0.53$ for the present-day universe. By contrast, fitting γΛCDM (i.e., ΛCDM with γ free) to CMB+$f\sigma_8$ data gives $\gamma = 0.639 \pm 0.025$ and $\Omega_{m0} = 0.308 \pm 0.007$, which together imply $f_0 = 0.471 \pm 0.015$ [139, 231]. This $\sim 4\sigma$ upward shift in γ relative to the GR expectation constitutes the growth-index tension and corresponds to a suppressed present-day growth rate ($f_0 \simeq 0.47$) relative to the Planck-ΛCDM expectation ($f_0 \sim 0.53$). By contrast, Λ_sCDM, at its sweet-spot $z_\dagger \sim 1.7$ and retaining the GR benchmark $\gamma \simeq 0.55$, with Planck-anchored $\Omega_{m0} \simeq 0.27$ [134–137], already predicts a suppressed present-day growth rate $f_0 \simeq 0.49$, closely matching the $f_0 \simeq 0.47$ inferred in γΛCDM analyses of CMB+$f\sigma_8$ data. Indeed, constraining $\gamma\Lambda_s$CDM (i.e., Λ_sCDM with free γ) with the same CMB+$f\sigma_8$ data yields $\gamma = 0.586 \pm 0.022$ and $\Omega_{m0} = 0.265 \pm 0.007$, implying $f_0 = 0.461 \pm 0.015$—in excellent agreement (within $\sim 0.5\sigma$) with the γΛCDM inference for f_0—while γ remains within $\sim 1.5\sigma$ of the GR value, thereby alleviating the growth-index tension [139]. In γΛCDM, the suppression of f_0 inferred from CMB+$f\sigma_8$ is achieved by raising the growth index to $\gamma \sim 0.64$, suggestive of a departure from GR, while keeping Ω_{m0} close to its Planck-ΛCDM

value. In $\gamma\Lambda_{\rm s}$CDM (with $z_\dagger \sim 1.7$), it arises chiefly from a lower matter density—$\Omega_{\rm m0}$ smaller by ~ 0.04 relative to Planck-ΛCDM—while the fitted $\gamma \sim 0.59$ remains statistically consistent with GR ($\gamma \simeq 0.55$).

Finally, halo-scale analyses based on spherical collapse in the *abrupt* $\Lambda_{\rm s}$CDM background show that bound structures survive the transition, and that the *virial overdensity* shifts relative to Planck-ΛCDM depending on whether the switch occurs before or after turnaround—that is, halos virialize with either increased or reduced overdensity contingent on the transition timing. This behavior encodes both the *duration* and *depth* of the pre-transition AdS phase, together with post-transition dS-like CC damping [140]. In this idealized limit, the transition manifests as a type II (sudden) singularity [232] at $z = z_\dagger$ [140]. Crucially, even in its most extreme, abrupt form, the mirror AdS-to-dS transition neither dissociates bound systems nor significantly perturbs Newtonian virialized halos, and this singularity, which already has mild dynamical impact, disappears once the transition is smoothed [140].[1]

Taken together, the linear-regime growth and halo-scale spherical-collapse results point to a concrete, falsifiable *nonlinear* signature characteristic of the $\Lambda_{\rm s}$CDM scenario. During the AdS-like CC era, reduced Hubble friction (relative to ΛCDM) seeds an early excess of power at high comoving wavenumbers k (units $h\,{\rm Mpc}^{-1}$). After the AdS-to-dS transition, $H(z)$ in the dS-like CC era closely tracks the ΛCDM redshift dependence but at higher values, thereby suppressing subsequent growth more efficiently than in ΛCDM. As nonlinearity propagates to progressively larger physical scales (i.e., as the nonlinear scale $k_{\rm NL}(z)$ decreases), the *maximum relative difference*, $P_{\Lambda_{\rm s}{\rm CDM}}/P_{\Lambda{\rm CDM}} - 1$, is expected to track $k_{\rm NL}(z)$. This appears as a *localized*, redshift-dependent crest in $P_{\Lambda_{\rm s}{\rm CDM}}/P_{\Lambda{\rm CDM}}$ that drifts to lower k with time. Unlike a scale-independent rescaling (e.g., of σ_8 or A_s), the crest's *amplitude* and *k-location* encode the integrated background history—how long and how strongly the Universe evolved in the AdS-like CC era, and how rapidly it was subsequently damped in the dS-like CC era. The crest is expected to arise near the AdS-to-dS transition, initially around $k_{\rm NL}(z_\dagger)$ with, for example, $z_\dagger \sim 1.7$, and then migrate, in comoving k, toward the group or poor-cluster regime by $z = 0$, where weak lensing, galaxy–galaxy lensing, cluster counts, and tSZ power are most sensitive. If the transition occurs earlier, for example $z_\dagger \sim 2.0$, the same morphology should be obtained but with reduced amplitude and earlier onset: the dark energy fraction is smaller at higher redshift, and the longer post-transition era provides more time to damp and redistribute the pre-transition excess, yielding a weaker residual feature by $z = 0$.

This work tests these predictions in the fully nonlinear regime using relativistic N-body simulations with `gevolution`. We simulate the *abrupt* $\Lambda_{\rm s}$CDM limit, a controlled proxy for a smooth but rapid transition, alongside a matched ΛCDM baseline, adopting two independent best-fit parameter sets (Planck-only and a combined "full" dataset; see Table I). Baryons and CDM are co-evolved as a single particle ensemble in a $(2080\,{\rm Mpc}/h)^3$ volume with $0.5\,{\rm Mpc}/h$ spatial resolution; a single massive neutrino with $\sum m_\nu = 0.06\,{\rm eV}$ is included in the matter sector and evolved linearly. We analyze the absolute matter power spectra up to $k_f \equiv k_{\rm Ny}/4 \simeq 1.6\,h\,{\rm Mpc}^{-1}$, and we track the localized feature in their relative behaviour down to $k \gtrsim 2\,h\,{\rm Mpc}^{-1}$, exploiting reduced sensitivity of the *ratio* $P_{\Lambda_{\rm s}{\rm CDM}}/P_{\Lambda{\rm CDM}}$ to resolution limits. Consistency in the linear regime is verified by cross-checking `gevolution` outputs against the Cosmic Linear Anisotropy Solving System (`CLASS`) in Newtonian gauge.

The paper is organized as follows. Following a review of the background dynamics and linear phenomenology of $\Lambda_{\rm s}$CDM in the Introduction (Section I), Section II introduces the abrupt $\Lambda_{\rm s}$CDM background and linear phenomenology, and details our simulation setup and validation. Section III presents the nonlinear power-spectrum results, quantifying the crest's amplitude and redshift-dependent k-drift, and mapping them to observational targets. Section IV summarizes the implications and outlines future tests.

II. BACKGROUND AND SIMULATION SETUP

To study the matter power spectrum in $\Lambda_{\rm s}$CDM relative to ΛCDM, we perform two sets of N-body simulations using the best-fit cosmological parameters from the *Planck*-only and full datasets listed in Table I. Simulations are carried out with the particle-mesh (PM) relativistic code `gevolution` [233, 234], which by default evolves perturbations in the Poisson gauge. Our use of `gevolution` is motivated by robustness and consistency: it provides a controlled GR framework in a well-defined gauge, evolves the metric potentials sourcing particle motion self-consistently, and allows a clean inclusion of relativistic species (here implemented linearly).

Massive neutrinos are included in the minimal-mass normal hierarchy with $\sum m_\nu = 0.06\,{\rm eV}$, implemented as a single massive eigenstate. Identical clustering is assumed for baryons and CDM (i.e., no bias), and our results do not incorporate baryonic feedback effects on small scales. Baryons and CDM are co-evolved in a single ensemble of 4160^3 particles, with initial perturbations generated from a weighted average of their separate transfer functions (the *blend* option in `gevolution`). All runs are performed

[1] For a smooth AdS-to-dS transition modeled with a DE field in GR, the type II singularity is absent. Because $p_{\rm DE}$ remains finite while $\rho_{\rm DE}$ crosses zero continuously at $z = z_\dagger$, the equation-of-state parameter $w_{\rm DE} \equiv p_{\rm DE}/\rho_{\rm DE}$ diverges there, $\lim_{z\to z_\dagger^\pm} w_{\rm DE}(z) = \pm\infty$, which, however, is a safe singularity: all background quantities (a, H, $\dot{H}$), as well as the total energy density and pressure, remain finite and continuous. In simple scalar-field realizations, the sound speed is luminal, $c_{\rm s}^2 = 1$. See Refs. [140, 173, 213] for details.

TABLE I. Best-fit cosmological parameters for the ΛCDM and $\Lambda_{\rm s}$CDM models used in our simulations. Values are derived from the parameter analyses of Ref. [136]: "Planck" corresponds to *Planck* CMB-only, while "Full" denotes the combined set *Planck*+$\mathrm{BAO_{tr}}$+PantheonPlus&SH0ES+KiDS-1000. The values listed are nearby best-fits obtained by locally re-optimizing around the posteriors of Ref. [136] (see Section II).

Parameter	ΛCDM (Planck)	ΛCDM (full)	$\Lambda_{\rm s}$CDM (Planck)	$\Lambda_{\rm s}$CDM (full)
$10^2\omega_b$	2.235	2.283	2.236	2.243
$\omega_{\rm cdm}$	0.1202	0.1143	0.1202	0.1192
$100\,\theta_*$	1.0418	1.0422	1.0417	1.0418
$\ln(10^{10}A_s)$	3.049	3.079	3.036	3.030
n_s	0.9658	0.9797	0.9648	0.9651
τ	0.0549	0.0771	0.0484	0.0485
$z_\dagger$	—	—	1.927	1.669
$\Omega_{\rm m}$	0.3163	0.2816	0.2872	0.2676
σ_8	0.8136	0.8076	0.8216	0.8238
H_0 [km s^{-1}Mpc^{-1}]	67.28	69.96	70.61	72.90
t_0 [Gyr]	13.80	13.71	13.62	13.53

in boxes of size $L = 2080\,\mathrm{Mpc}/h$ with 4160 grid points. Additional parameters not shown in Table I include $N_{ur} = 2.0328$ for two ultra-relativistic neutrinos and $T_\nu/T_\gamma = 0.71611$, which are common to both cosmological models.

Outputs for ΛCDM and $\Lambda_{\rm s}$CDM cosmologies are directly comparable, since all runs within a given dataset (*Planck*-only vs. full) share identical simulation and IC (initial conditions) generation settings. The code employs a Fast Fourier Transform (FFT) algorithm and therefore operates at fixed resolution. However, limitations associated with the fixed lattice are partially mitigated when considering the *ratios* $P_{\Lambda_{\rm s}\rm CDM}/P_{\Lambda\rm CDM}$, which remain sufficiently reliable for our purposes beyond the k-range adopted for the individual absolute spectra $P_{\Lambda_{\rm s}\rm CDM}$ and $P_{\Lambda\rm CDM}$.

Initial perturbation amplitudes at $z_{\rm ini} = 100$ are generated with the Boltzmann code `CLASS` [235]. In the simulations, metric evolution includes massive-neutrino perturbations only at linear order, in contrast to the joint CDM-baryon component (hereafter denoted cb), which is represented by an N-body ensemble. Time-dependent neutrino transfer functions are provided by `CLASS` at runtime [236, 237].

The codes are left unaltered for ΛCDM. For $\Lambda_{\rm s}$CDM, we modify only the *background* evolution in both `gevolution` and `CLASS` to implement a non-clustering, sign-switching cosmological constant $\Lambda_{\rm s}$. In this framework, the standard cosmological constant Λ of the ΛCDM model is replaced by $\Lambda_{\rm s}$, which undergoes a rapid sign switch near $z_\dagger$, with an AdS-like phase ($\Lambda_{\rm s} < 0$) at earlier times and a dS-like phase ($\Lambda_{\rm s} > 0$) thereafter. We adopt the idealized step-limit prescription

$$\Lambda_{\rm s}(z) = \Lambda_{\rm s0}\,\mathrm{sgn}(z_\dagger - z)\,, \tag{1}$$

where sgn denotes the signum function [134–136]. This choice modifies only the background expansion (i.e. no dark energy clustering) and serves as a simplifying approximation to a fast but continuous sign switch. The Friedmann equation then reads

$$\frac{H^2}{H_0^2} = \Omega_{\rm r0}(1+z)^4 + \Omega_{\rm m0}(1+z)^3 + \Omega_{\Lambda_{\rm s}0}\,\mathrm{sgn}(z_\dagger - z)\,. \tag{2}$$

The present-day density parameters retain their standard definitions (setting $c \equiv 1$) $\Omega_{\rm r0} = 8\pi G\,\varepsilon_{\rm r0}/(3H_0^2)$, $\Omega_{\rm m0} = 8\pi G\,\varepsilon_{\rm m0}/(3H_0^2)$, and $\Omega_{\Lambda_{\rm s}0} = \Lambda_{\rm s0}/(3H_0^2)$. On sub-horizon scales, the pressureless linear growth still satisfies [135]

$$\ddot{\delta} + 2H\dot{\delta} - 4\pi G\rho_m\,\delta = 0\,. \tag{3}$$

For the baseline free parameters we rely on the recent global analysis of $\Lambda_{\rm s}$CDM in Ref. [136], which identifies a transition at $z_\dagger \simeq 1.7$–1.9 and reports improvements across multiple data combinations relative to ΛCDM.

It has been shown in Ref. [238] that in `gevolution` simulations carried out in the Poisson gauge, the impact of early radiation on the matter power spectrum—specifically on very large scales—remains at the sub-percent level. Motivated by this, we include photon and massless-neutrino perturbations only down to $z = 15$. Their transfer functions are computed with `CLASS` and supplied to `gevolution` at runtime to construct the corresponding density fields (analogous to the treatment of massive neutrinos). At later times, down to $z = 0$, these species are retained only in the background evolution.

The entries in Table I are point estimates obtained by locally re-optimizing the likelihood around the MontePython chains of Ref. [136] for the two datasets employed here: "Planck" (Planck CMB only) and "full" (the combined *Planck*+$\mathrm{BAO_{tr}}$+PantheonPlus&SH0ES+KiDS-1000 analysis). Ref. [136] sampled parameters with `CLASS`+MontePython (Metropolis-Hastings, $R - 1 < 10^{-2}$) and reported 68% CL posteriors and best fits; our local re-optimization yields nearby best fits consistent with those posteriors. Small numerical shifts relative to Ref. [136] are immaterial and leave all figures unchanged at the precision shown.

Throughout, "total matter" denotes the sum of baryons, CDM, and massive neutrinos. Comparisons to linear theory are performed with `CLASS` in Newtonian gauge (the gauge choice is discussed below).

III. RESULTS AND INTERPRETATION

Fig. 1 presents the total-matter power spectra at $z = 15, 2, 1, 0$ for both cosmologies, using the *Planck*-only (left) and full (right) best-fit parameter sets in Table I. Approaching $k \sim \mathcal{O}(1)\,h\,\mathrm{Mpc}^{-1}$, at very high redshift ($z = 15$), the two models are nearly indistinguishable, as expected when the the dark energy fraction is negligible ($\Omega_\Lambda \simeq |\Omega_{\Lambda_{\rm s}}| \approx 0$); the small residual offset in power reflects the different late-time best fits (e.g., A_s, n_s, $\Omega_{\rm m0}$). At lower redshift, in the nonlinear regime of interest ($k \gtrsim 0.1\,h\,\mathrm{Mpc}^{-1}$), the largest *relative* difference appears in the neighborhood of the sign-switch (*mirror* AdS-to-dS

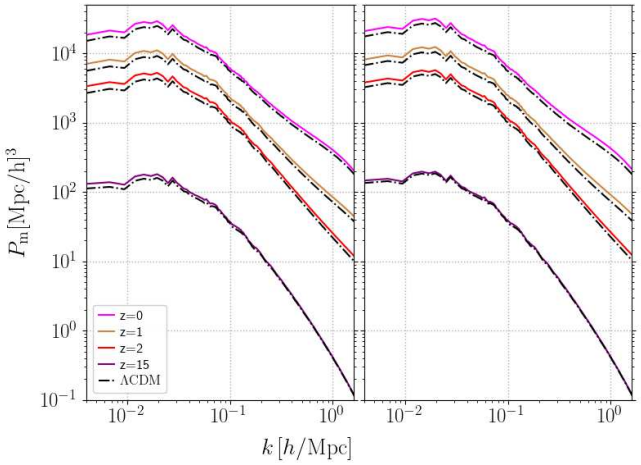

FIG. 1. Total-matter (baryons+CDM+massive ν) power spectra from our `gevolution` simulations, shown for the *Planck*-only (left) and full (right) best-fit parameter sets at $z = 15, 2, 1, 0$. Colored solid curves correspond to $\Lambda_{\rm s}$CDM, while black dash-dotted curves indicate ΛCDM. Within each dataset, both runs share identical simulation and IC generation settings. Absolute spectra are plotted up to $k_{\rm f} = 1.6\,h\,{\rm Mpc}^{-1} \simeq k_{\rm Ny}/4$.

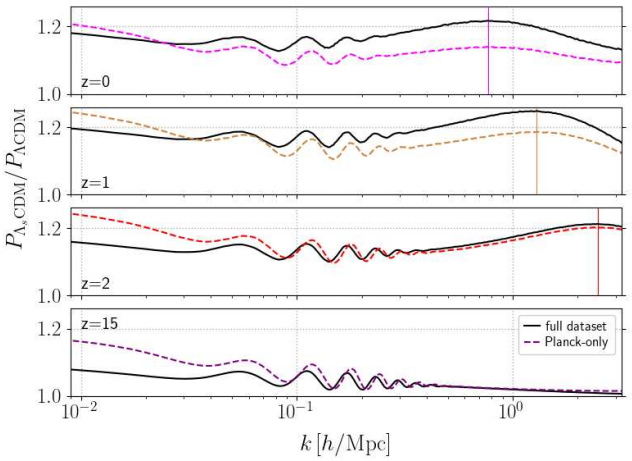

FIG. 2. Ratios of the total-matter power spectra, $P_{\Lambda_{\rm s}{\rm CDM}}/P_{\Lambda{\rm CDM}}$, at $z = 15, 2, 1, 0$ for the *Planck*-only (dashed) and full (solid) best-fit parameter sets. Vertical tick marks denote the k-locations of the local maxima from $z = 2$ onward. Peak amplitudes are: *Planck*-only, 1.202 at $z = 2$, 1.186 at $z = 1$, 1.140 at $z = 0$; full dataset, 1.212 at $z = 2$, 1.248 at $z = 1$, 1.217 at $z = 0$.

transition) epoch and follows the dataset-dependent $z_\dagger$: for the *Planck*-only case it is maximal at $z \simeq 2$ (just before $z_\dagger \simeq 1.93$), whereas for the full dataset it is maximal at $z \simeq 1$ (consistent with $z_\dagger \simeq 1.67$). This behavior is made explicit in Fig. 2, which shows the ratios $P_{\Lambda_{\rm s}{\rm CDM}}/P_{\Lambda{\rm CDM}}$ at the same four redshifts. The enhancement peaks at wavenumbers $k \simeq 1$–$3\,h\,{\rm Mpc}^{-1}$ with amplitudes of order 20–25% (precisely: 1.202 at $z = 2$ for *Planck*-only; 1.248 at $z = 1$ for the full dataset), i.e., within the wavelength interval $\lambda = 2\pi/k \simeq 2.1$–$6.3\,h^{-1}{\rm Mpc}$ where nonlinear collapse is most efficient. After the sign switch, i.e., in the dS-like CC era ($z < z_\dagger$), the relative excess diminishes but does not vanish: by $z = 0$, the crest has migrated to larger physical scales, with its peak at $k \simeq 0.8\,h\,{\rm Mpc}^{-1}$ and amplitudes of 1.140 (*Planck*-only) and 1.217 (full). In other words, the peak amplitude declines from $\sim$20% at $z = 2$ to $\sim$ 14% at $z = 0$ for the *Planck*-only case, and from $\sim$25% at $z = 1$ to $\sim$22% at $z = 0$ for the full dataset. The vertical tick marks in Fig. 2 indicate the k-locations of the local maxima at each redshift; these are essentially insensitive to small parameter differences *within* each dataset, confirming that the peak's position is controlled by the dynamical history (i.e., the timing of the mirror AdS-to-dS transition) rather than by mild shifts in (Ω_{m0}, H_0, A_s, n_s).

The absolute spectra in Fig. 1 are shown only up to $k_{\rm f} = 1.6\,h\,{\rm Mpc}^{-1}$, defined as one quarter of the Nyquist frequency, $k_{\rm Ny} = \pi/({\rm resolution}) \simeq \pi/0.5 \simeq 6.3\,h\,{\rm Mpc}^{-1}$. The leading-order discretization error relative to the continuum prediction, $P_{\rm continuum}$, partly cancels in the *ratios* $P_{\Lambda_{\rm s}{\rm CDM}}/P_{\Lambda{\rm CDM}}$, as discussed around Eq. (5.1) of Ref. [236], making them less sensitive to the limitations of fixed resolution. Accordingly, in Fig. 2 we report the locations and amplitudes of the maxima at $z = 2$ even though they lie slightly beyond $k_{\rm f}$. These should be regarded as robust *relative* features, while absolute amplitudes beyond $k_{\rm f}$ are not interpreted further here.

Figures 3 (*Planck*-only) and 4 (full dataset) compare the cb-only power spectra from N-body runs (solid) to the corresponding linear predictions from `CLASS` (black dash-dotted). As noted earlier, although the cb component shown separately here *excludes* massive ν, their perturbations still source the metric linearly. On large, linear scales ($k \lesssim 0.1$–$0.2\,h\,{\rm Mpc}^{-1}$) the agreement between `gevolution` and `CLASS` is excellent at all redshifts, validating the consistent implementation of the modified background in the $\Lambda_{\rm s}$CDM cosmology across both codes. We emphasize that in `CLASS` we work in Newtonian gauge, since calculations in the default synchronous gauge are sensitive to the step in $H(z)$ for the abrupt $\Lambda_{\rm s}$CDM model. Meanwhile, our interpretation of the linear-theory versus simulation comparison focuses on subhorizon modes, $k \gtrsim 0.02\,h\,{\rm Mpc}^{-1}$, where finite-volume effects are negligible and gauge effects are no longer significant. For a complementary benchmark against an analytic nonlinear prescription (`HMCode`) and an estimate of its range of validity in this setting, see Appendix A (Figs. 7 and 8). Toward smaller scales the N-body spectra exceed the linear curves at low redshift, as expected from nonlinear growth. The corresponding *ratios* in Figs. 5 and 6 show the same trend: linear-theory ratios remain smooth and modest, whereas their N-body counterparts develop a localized crest around $k \sim \mathcal{O}(1)\,h\,{\rm Mpc}^{-1}$ at $z = 2, 1, 0$ (earlier and weaker for the *Planck*-only fit, later and stronger for the full dataset), confirming that the enhancement is

a genuine nonlinear response to the Λ_sCDM background.

A scale-independent change to the linear normalization (e.g., tuning σ_8 or A_s) cannot reproduce the *localized*, redshift-dependent crest that we find in the simulation ratio $P_{\Lambda_s\mathrm{CDM}}/P_{\Lambda\mathrm{CDM}}$ (Figs. 2, 5, 6). In our results the excess is confined to $k \sim \mathcal{O}(1)\,h\,\mathrm{Mpc}^{-1}$ and its peak shifts to larger physical scales (i.e., smaller comoving k) toward $z = 0$, reaching $k \simeq 0.6$–$1.0\,h\,\mathrm{Mpc}^{-1}$, while large scales remain consistent with linear-theory predictions in Newtonian (Poisson) gauge (cf. Figs. 3-4). A uniform amplitude change would affect all k similarly and cannot generate a drifting, localized crest; the feature is therefore *dynamical*, tracing the sign-switch (the mirror AdS-to-dS transition in Λ_s) history of $H(z)$ rather than a static renormalization of the spectrum.

Physical origin of the Λ_sCDM–ΛCDM deviations across redshift

The pattern we observe follows directly from how the presence of a rapid mirror AdS-to-dS transition in the late universe ($z_\dagger \sim 2$) reshapes the Hubble friction term in the (subhorizon, pressureless) linear growth equation given Eq. (3), together with subsequent nonlinear mode coupling. At very high redshift ($z \gtrsim 3.5$), the dark energy fraction is negligible $\Omega_\Lambda(z \gtrsim 3) \simeq |\Omega_{\Lambda_s}(z \gtrsim 3)| \lesssim \mathcal{O}(10^{-2})$, so Λ_sCDM and ΛCDM are practically indistinguishable near $k \sim \mathcal{O}(1)\,h\,\mathrm{Mpc}^{-1}$. The small offsets seen at $z = 15$ are indirect, tracing parameter reoptimization (e.g., A_s, n_s, Ω_{m0}) that fix the growth normalization and transfer-function shape at the initial redshift (cf. Figs. 1, 3, 4). Approaching the transition from above ($z_\dagger < z \lesssim 3.5$), the effective CC is AdS-like ($\Lambda_s < 0$), the expansion rate is lowered at fixed (Ω_m, Ω_r), the friction piece $2H\dot{\delta}$ is reduced, and the linear growth factor is temporarily enhanced during this window ($D_{\Lambda_s}/D_\Lambda > 1$). In the simulations, this manifests as a localized, scale-dependent boost peaking near the mirror AdS-to-dS transition, consistent with the dataset-dependent $z_\dagger$ (see the total-matter and cb ratios in Figs. 2, 5, 6).

After the transition ($z < z_\dagger$), the effective CC is dS-like ($\Lambda_s > 0$) as in ΛCDM, but the best-fit Λ_sCDM backgrounds (both the *Planck*-only and full) feature a larger late-time expansion rate, which increases Hubble friction and partially suppresses subsequent growth. Crucially, this acts on a field that was already amplified during the AdS-like effective CC phase ($\Lambda_s < 0$), so the imprint cannot be erased. Nonlinear evolution then transfers part of the excess toward larger physical scales: in Fourier space, the crest in P_{Λ_s}/P_Λ migrates from $k \simeq 2$–$3\,h\,\mathrm{Mpc}^{-1}$ ($k \simeq 1$–$2\,h\,\mathrm{Mpc}^{-1}$ for the full dataset) near the transition to $k \simeq 0.6$–$1.0\,h\,\mathrm{Mpc}^{-1}$ by $z = 0$,[2] consistent with mode coupling and the evolving one-halo–two-halo balance. The comoving length that corresponds to the top of this crest, $\ell = 2\pi/k \simeq 8\,h^{-1}\mathrm{Mpc}$, after mean-density top-hat mapping (whose response peaks near $kR \simeq \pi$), translates to $R \simeq \pi/k \simeq 4\,h^{-1}\mathrm{Mpc}$ and yields a characteristic mass $M(R) \equiv (4\pi/3)\,\bar{\rho}_m\,R^3 \sim$ few $\times\, 10^{13}\,h^{-1}M_\odot$ with $\bar{\rho}_m = \Omega_{\mathrm{m0}}\rho_{\mathrm{c0}}$. Across the crest, i.e., $k \simeq 0.6$–$1.0\,h\,\mathrm{Mpc}^{-1}$, we get $R \simeq 3.1$–$5.2\,h^{-1}\mathrm{Mpc}$ and $M \simeq (1.5$–$6.8)\times 10^{13}\,M_\odot$, $M \simeq (1.3$–$6.1)\times 10^{13}\,M_\odot$ for the *Planck*-only and full dataset, respectively, i.e., group or poor-cluster scales. We

[2] This interval roughly brackets a flat top at $z = 0$ in Fig. 2 for both datasets, with the local maxima near $k \simeq 0.8\,h\,\mathrm{Mpc}^{-1}$ in both total-matter and cb ratios (Figs. 2, 5, 6).

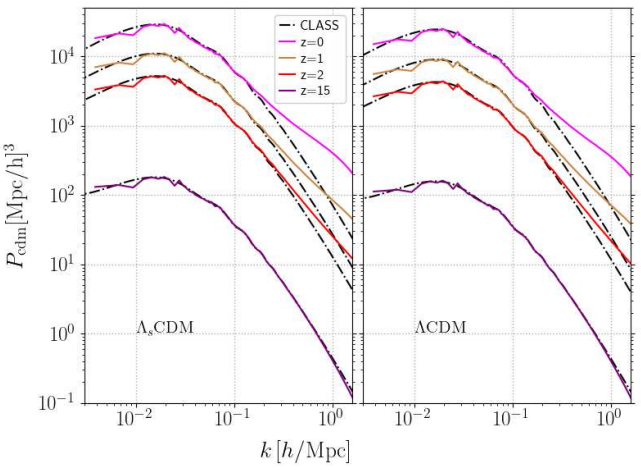

FIG. 3. CDM-baryon (cb) power spectra from `gevolution` at $z = 15, 2, 1, 0$ for the *Planck*-only best-fit parameters. Dash-dotted curves show the corresponding *linear* predictions from `CLASS` in Newtonian gauge. Agreement is excellent on large scales, while deviations at higher k reflect nonlinear clustering for $z \leq 2$.

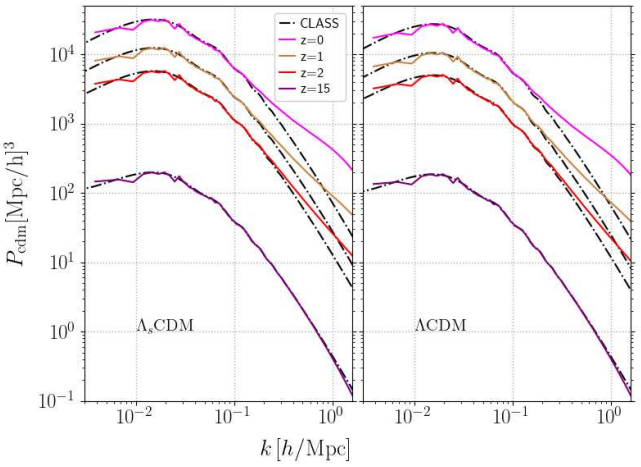

FIG. 4. CDM-baryon (cb) power spectra from `gevolution` at $z = 15, 2, 1, 0$ for the full best-fit parameters. Dash-dotted curves show the corresponding *linear* predictions from `CLASS` in Newtonian gauge. As in the *Planck*-only case, excellent agreement is found on large scales between each N-body and linear prediction pair.

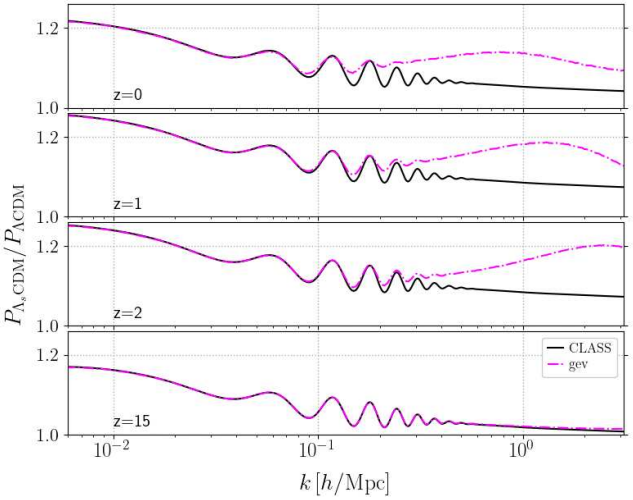

FIG. 5. Ratios of CDM–baryon (cb) power spectra, $P_{\Lambda_s\mathrm{CDM}}/P_{\Lambda\mathrm{CDM}}$, at $z = 15, 2, 1, 0$ for the *Planck*-only best-fit parameters. A localized enhancement appears near the switch epoch and subsequently drifts to larger physical scales, reaching $k \sim 0.6$–$1.0\,h\,\mathrm{Mpc}^{-1}$ by $z = 0$. On linear scales the relative spectra from simulations agree with those from `CLASS`, as expected.

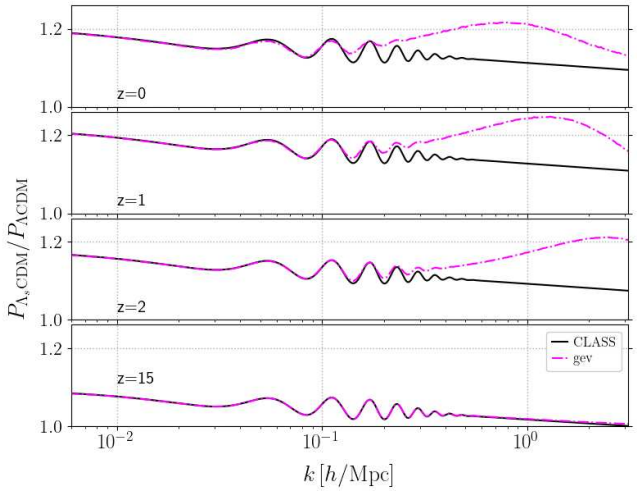

FIG. 6. Ratios of CDM-baryon (cb) power spectra, $P_{\Lambda_s\mathrm{CDM}}/P_{\Lambda\mathrm{CDM}}$, at $z = 15, 2, 1, 0$ for the full best-fit parameters. As in the *Planck*-only case, a localized enhancement emerges near the switch epoch and drifts to larger physical scales by $z = 0$ ($k \sim 0.6$–$1.0\,h\,\mathrm{Mpc}^{-1}$). In the linear regime the simulation ratios agree with those from `CLASS`.

emphasize that $M(R)$ here is a *characteristic linear scale* defined from the *background* matter density; virial halo masses at these radii are larger because collapsed regions have overdensities $\Delta \gg 1$ (tens to hundreds), and their virial radii ($R_{\mathrm{vir}} \sim R\,\Delta^{-1/3}$) are correspondingly smaller than R. We do not quote a more precise M because the mapping depends on the chosen window and on halo definitions; the key point is that the affected modes lie in the group or poor-cluster regime, precisely the scales most relevant for galaxy-galaxy lensing, small-scale shear, cluster counts and tSZ statistics. For reference, σ_8 is the root-mean-square (rms) of the *linear* matter field today smoothed with a top-hat of radius $8\,h^{-1}$Mpc, whereas the crest we discuss lies at the smaller scale $R \simeq 4\,h^{-1}$Mpc.

Overall, the figures show a coherent causal chain: parameter-driven, percent-level offsets only where the effective CC sector is irrelevant; a genuine dynamical enhancement tied to the AdS-like effective CC window; and a persistent, drifting crest thereafter, viz., in the dS-like CC era, seen clearly in both the total-matter and cb-only spectra, which are consistent with linear theory on large scales and underscore the robustness of this interpretation.

Connection to cosmic noon and observational tests

Observational reconstructions place the cosmic star-formation-rate density (SFRD) peak at $z \simeq 1.5$–2 (see, e.g., [239]). In standard ΛCDM, its timing and amplitude emerge from the interplay of halo assembly, gas accretion, cooling and metal enrichment, and feedback; gravity sets the large-scale preconditions but does not by itself fix the peak. In this context, our simulations show that Λ_sCDM supplies a stronger gravitational backdrop near the relevant epoch for *both* data combinations. The maximum near $z \sim 2$ for the *Planck*-only fit, for instance, appears at $k \simeq 2$–$3\,h\,\mathrm{Mpc}^{-1}$. As worked out in detail in the previous subsection, this interval maps to $R \simeq 1.0$–$1.6\,h^{-1}$Mpc and hence to $M(R) \sim 10^{11}$–$10^{12}\,M_\odot$. For *collapsed* halos, the corresponding virial masses are pushed to $M_{\mathrm{vir}} \sim 10^{13}$–$10^{14}\,M_\odot$, i.e., the range widely believed to dominate the SFRD.

The localized boost at $k \sim 1$–$3\,h\,\mathrm{Mpc}^{-1}$ near $z \sim 1$–2 aligns with the broader "cosmic noon" picture: these modes correspond to the group and cluster halo regime where rapid *halo growth*, *compaction and quenching*, and *black-hole accretion* are observed to peak, with the SFRD maximized at similar epochs (e.g., [239–243]). The same k range is also where *thermal Sunyaev–Zel'dovich (tSZ)* and *galaxy–galaxy lensing* and *cosmic shear* measurements have their highest sensitivity [244–247]. We emphasize that cosmic noon itself is not a tension for ΛCDM once baryonic physics is modeled; rather, our result, in Λ_sCDM, provides a *gravitational prior* that can modestly modulate collapse efficiencies near that epoch. While detailed outcomes (quenching pathways, size growth, AGN duty cycles) are baryon-controlled and beyond the scope of our dark-matter-only simulations, the predicted redshift-dependent and *localized* power excess offers a concrete near-term target for hydrodynamical simulations and for small-scale lensing and tSZ analyses.

IV. CONCLUSION

We have presented the results of relativistic N-body simulations showing how replacing the standard cosmological constant Λ of ΛCDM with a sign-switching cosmological constant [133–136], $\Lambda_{\rm s}$—which undergoes a rapid mirror AdS-to-dS transition in the late universe (at redshift $z_\dagger \sim 2$)—modifies structure growth in the nonlinear regime, using `gevolution` with an *abrupt* $\Lambda_{\rm s}$CDM [134–136] background under general relativity and two independent best-fit parameter sets (*Planck* CMB-only and the "full" combination). While $\Lambda_{\rm s}$CDM and ΛCDM are observationally indistinguishable at $z \gtrsim 3$ on $k \sim \mathcal{O}(1)\,h\,{\rm Mpc}^{-1}$, the AdS-like CC ($\Lambda_{\rm s} < 0$) phase for $z_\dagger < z \lesssim 3$ reduces Hubble friction and *dynamically* amplifies the growth of matter perturbations. After the sign switch ($z < z_\dagger$), the CC is dS-like ($\Lambda_{\rm s} > 0$) and the late-time expansion rate is larger than in ΛCDM, partially suppressing subsequent growth but not erasing the pre-amplified field. In Fourier space, this causal sequence yields a localized, redshift-dependent excess: a crest in $P_{\Lambda_{\rm s}{\rm CDM}}/P_{\Lambda{\rm CDM}}$ that peaks near the transition at $k \simeq 1$–$3\,h\,{\rm Mpc}^{-1}$ with a fit-dependent amplitude of $\simeq 1.20$–1.25, advected to larger physical scales with time, leaving a robust 15–20% uplift at $z = 0$ around $k \simeq 0.6$–$1.0\,h\,{\rm Mpc}^{-1}$ (Figs. 1, 2). In both absolute and relative cb-only spectra, large-scale results agree with linear predictions (Figs. 3–6), where `CLASS` comparisons are performed in Newtonian gauge.

The affected wavenumbers correspond to physically distinct, observationally accessible regimes. For the *Planck*-only data (full dataset), near the transition epoch $z \sim 2$ ($z \sim 1$), the interval $k \simeq$ 2-3 $h\,{\rm Mpc}^{-1}$ ($k \simeq$ 1-2 $h\,{\rm Mpc}^{-1}$) maps to $R \simeq \pi/k \simeq$ 1.0-1.6 h^{-1}Mpc ($R \simeq$ 1.6-3.1 h^{-1}Mpc) and a *characteristic Lagrangian* mass $M(R) \simeq 5.4 \times 10^{11}$-$1.8 \times 10^{12}\,M_\odot$ ($M(R) \simeq 1.6 \times 10^{12}$-$1.3 \times 10^{13}\,M_\odot$) from the mean-density top-hat relation. Interpreted in terms of *collapsed* halos (e.g., $M_{200{\rm c}}$ or $M_{500{\rm c}}$), the same modes correspond to group-cluster systems with $M \sim 10^{13}$-$10^{14}\,M_\odot$ ($M \sim 10^{14}$-$10^{15}\,M_\odot$) once typical virial overdensities $\Delta \sim$ 100-200 are included; this is precisely the mass range widely believed to dominate the SFRD at "cosmic noon." By $z = 0$, the migrating crest sits at $k \simeq$ 0.6-1.0 $h\,{\rm Mpc}^{-1}$ (comoving scales $\ell = 2\pi/k \simeq$ 6-10 h^{-1}Mpc), which corresponds to $R \simeq$ 3.1-5.2 h^{-1}Mpc and $M(R) \simeq$ (1.5-6.8) $\times 10^{13}\,M_\odot$, $M(R) \simeq$ (1.3-6.1) $\times 10^{13}\,M_\odot$ for the *Planck*-only and full dataset, respectively, i.e., group or poor-cluster environments. Unlike a scale-independent shift in the fluctuation summaries σ_8 or S_8 (which largely act as global rescalings), $\Lambda_{\rm s}$CDM predicts a *shape* feature: a localized, redshift-dependent crest whose k-location tracks $z_\dagger$ and drifts to larger physical scales with time. Within a given redshift slice, the *Planck*-only and full-dataset runs place the local maxima at nearly the same k (Fig. 2); their differences lie primarily in the crest's *amplitude* and in which slice shows the strongest signal (earlier for *Planck*-only, later for full), consistent with their different $z_\dagger$. This signature, if present, should manifest as a localized excess in small-scale cosmic shear and galaxy-galaxy lensing, a tilt in the tSZ power around group scales, and modest, redshift-dependent changes in the abundance and internal structure of halos in the 10^{13}-$10^{15}\,M_\odot$ range.

Our analysis excludes baryonic physics and scenarios beyond $\sum m_\nu = 0.06\,{\rm eV}$ in the form of a single massive neutrino. Small-scale amplitudes of the absolute power spectra should be interpreted with caution due to the fixed simulation resolution; accordingly, we show them only up to $k_f \equiv k_{\rm Ny}/4$. Their *ratios*, however, remain informative somewhat beyond k_f, enabling us to track the emergence of localized features down to $k \gtrsim 2\,h\,{\rm Mpc}^{-1}$. Linear-regime cross-checks further strengthen the robustness of our findings, in particular the consistent implementation of the $\Lambda_{\rm s}$CDM background in the N-body framework.

Looking ahead, hydrodynamical simulations and a systematic exploration of $\sum m_\nu$ are required to propagate the crest's amplitude and k-drift into fully marginalized constraints on $(z_\dagger, \Omega_{\Lambda_{\rm s}0})$. On the observational side, a combined analysis of small-scale weak lensing, galaxy-galaxy lensing, cluster counts, and tSZ power offers a sharp test: detecting, or ruling out, a redshift-evolving, localized excess in power at $k \sim \mathcal{O}(1)\,h\,{\rm Mpc}^{-1}$ would provide a direct probe of whether late-time cosmic acceleration prefers a sign-switching cosmological constant. In this sense, $\Lambda_{\rm s}$CDM [133–136] provides a well-defined benchmark for forthcoming precision probes such as *Euclid*, LSST, and CMB-S4, where small-scale lensing and cluster observables will be key to confirming or excluding a sign-switching vacuum sector.

Another natural direction is to extend our N-body program beyond the abrupt $\Lambda_{\rm s}$CDM [134–136] approximation adopted under GR. While the abrupt limit provides a clean proof of concept, a fully consistent realization of the scenario calls for a *smooth* transition, replacing the instantaneous sign switch with a well-defined dynamical process. Phenomenologically, this can be modeled with sigmoid-like histories for $\Lambda_{\rm s}(z)$ (e.g., hyperbolic tangents) in redshift (or scale factor), controlled by a rapidity parameter η that governs the duration and sharpness of the mirror AdS-to-dS transition (see, e.g., [219, 222]). One can simulate such smooth families (characterized by $(z_\dagger, \eta)$) within GR and map this two-parameter space onto the crest's amplitude and k-drift in $P_{\Lambda_{\rm s}{\rm CDM}}/P_{\Lambda{\rm CDM}}$, thereby testing how the *duration*/*rapidity* and functional form of the transition modulate the localized nonlinear signature. Beyond this phenomenological step, a more fundamental route is to realize the transition via explicit microphysics within GR. A concrete example is Ph-$\Lambda_{\rm s}$CDM, where a phantom field with a hyperbolic tanh-type potential generates smooth mirror AdS-to-dS transitions and, more generally, asymmetric ones; in this GR framework one expects the growth index to remain near the GR benchmark, $\gamma \simeq 0.55$ [213, 248]. One can also investigate modified gravity embeddings of $\Lambda_{\rm s}$CDM, in which transient deviations of γ can arise around the transition epoch. Representative cases include $\Lambda_{\rm s}$VCDM

(a type-II minimally modified gravity) [137, 194] and $f(T)$-$\Lambda_{\rm s}$CDM in teleparallel gravity [209] (see also Ref. [206]). A systematic comparison across these realizations would clarify whether the same small-scale crest favored by data also selects a finite transition duration/rapidity and, if present, a controlled departure from GR confined to the transition epoch. Finally, there exist theoretical constructions of the *abrupt* scenario itself. $\Lambda_{\rm s}$CDM$^+$ provides a string-inspired realization that predicts a modest excess in the total effective number of relativistic species, $N_{\rm eff} \simeq 3.294$ [191, 193, 205], offering an orthogonal handle via early-time observables (CMB damping tail, BBN). It would also be interesting to explore $\Lambda_{\rm s}$CDM$_\pm$ [214], which extends $\Lambda_{\rm s}$CDM$^+$ by allowing the AdS-like CC to have variable depth (as also natural in the Ph–$\Lambda_{\rm s}$CDM framework [213]). Such generalizations introduce a degeneracy between the transition redshift and the AdS depth, but they predict richer dynamics in the nonlinear growth regime; in particular, sufficiently large negative AdS values could impact earlier epochs of cosmic history, potentially even before recombination. Both avenues furnish complementary tests: any detection (or null result) of a redshift-evolving, localized crest in the late-time matter power spectrum can be cross-checked against these early-time signatures, tightening the overall assessment of the $\Lambda_{\rm s}$CDM framework.

ACKNOWLEDGMENTS

The authors are grateful to Julian Adamek for insightful comments and valuable suggestions. They also thank Emre Özülker for fruitful discussions during the initial stages of this work. Finally, they thank Merab Gogberashvili for drawing their attention to the redshift of the peak in the cosmic star-formation rate. Ö.A. acknowledges the support by the Turkish Academy of Sciences in scheme of the Outstanding Young Scientist Award (TÜBA-GEBİP). E.D.V. is supported by a Royal Society Dorothy Hodgkin Research Fellowship. This work was partially supported by the Center for Advanced Systems Understanding (CASUS), financed by Germany's Federal Ministry of Education and Research (BMBF) and the Saxon state government out of the State budget approved by the Saxon State Parliament. Computing resources used in this work were provided by the high-performance computer at the NHR Center of TU Dresden, jointly supported by the Federal Ministry of Education and Research and the state governments participating in the NHR (www.nhr-verein.de/unsere-partner). This article is based upon work from COST Action CA21136 Addressing observational tensions in cosmology with systematics and fundamental physics (CosmoVerse) supported by COST (European Cooperation in Science and Technology).

DATA AVAILABILITY

Datasets generated to produce the matter power spectra analyzed in this work are publicly available in the Rossendorf Data Repository (RODARE) and may be accessed via doi.org/10.14278/rodare.4019 [249].

Appendix A: Benchmark against nonlinear prescriptions: `HMCode`

For completeness, we also consider nonlinear corrections to the CDM-baryon power spectrum predictions for all four cases studied in the manuscript using the `CLASS` implementation of `HMCode` [250]. Fig. 7 shows the ratios $P_{\Lambda_{\rm s}{\rm CDM}}/P_{\Lambda{\rm CDM}}$ at $z = 2, 1$ and 0 for both the *Planck*-only and full-dataset best-fit parameters [panels (a) and (b), respectively]. Results from `HMCode` agree well with those from N-body simulations with `gevolution` on mildly nonlinear to nonlinear scales, with the remaining differences at the sub-percent level for all redshifts up to $k \simeq 1\,h\,{\rm Mpc}^{-1}$. For $z = 2$, the difference stays below 1% throughout, whereas at $z = 1$ and 0 it reaches $\sim 3\%$ ($\sim 4\%$) around $k_{\rm max} = 3\,h\,{\rm Mpc}^{-1}$ for the *Planck*-only ("full") best-fit parameter set.

In Fig. 8, we switch to the *absolute* spectra and investigate how the cb-only results from N-body simulations compare to `HMCode` for ΛCDM and $\Lambda_{\rm s}$CDM cosmologies, separately, again for the *Planck*-only and full-dataset parameter sets [panels (a) and (b), respectively]. We observe strong consistency in how `HMCode` performs for the two models: down to the limit $k_{\rm f} = 1.6\,h\,{\rm Mpc}^{-1}$ that we adopt for the absolute spectra, the ΛCDM and $\Lambda_{\rm s}$CDM curves agree within 0.5% at $z = 2$ and 1 (only for the "full" dataset parameters this reaches $\sim 1\%$ at $z = 1$). At $z = 0$, the difference remains below 2% for each parameter set.

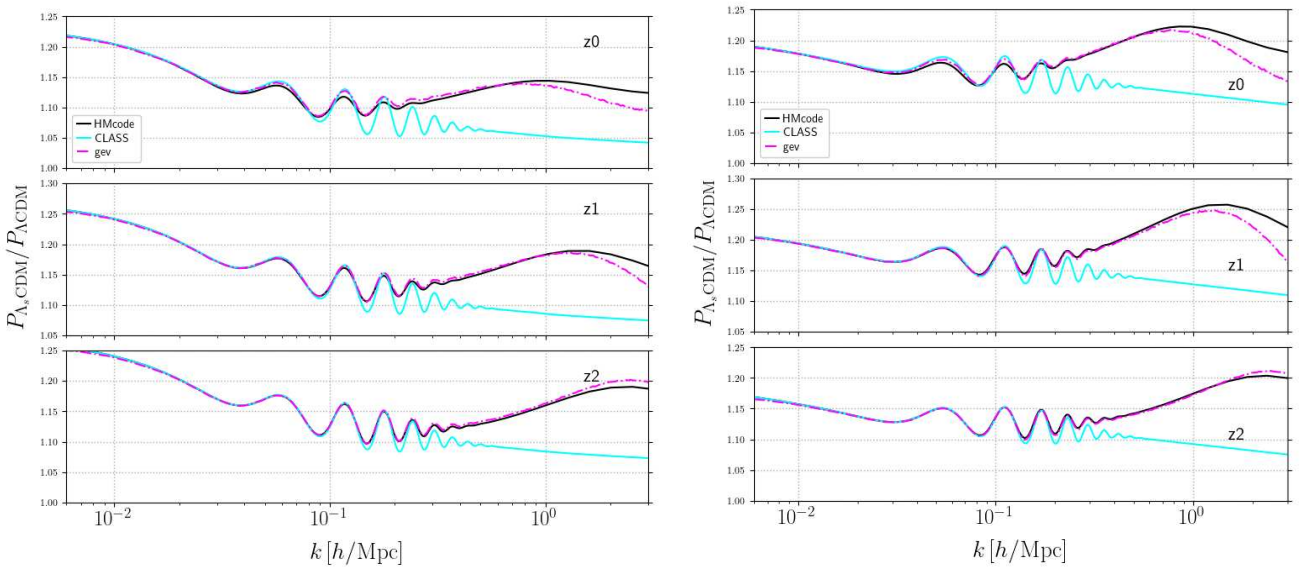

(a) *Planck*-only (b) full-dataset

FIG. 7. $P_{\Lambda_s\mathrm{CDM}}/P_{\Lambda\mathrm{CDM}}$ from `gevolution`, `CLASS`, and `HMCode` (implemented in `CLASS`) for (a) the *Planck*-only and (b) the full-dataset best-fit parameters, at $z = 2, 1$, and 0. The CDM-baryon (cb-only) curves from the N-body results are shown in Poisson gauge, whereas those from `CLASS` and `HMCode` are the synchronous-gauge spectra on linear scales (`CLASS` calculations are still performed in Newtonian gauge as in the main text). This does not affect our direct comparison at the redshifts of interest for $k \gtrsim 0.02\,h\,\mathrm{Mpc}^{-1}$.

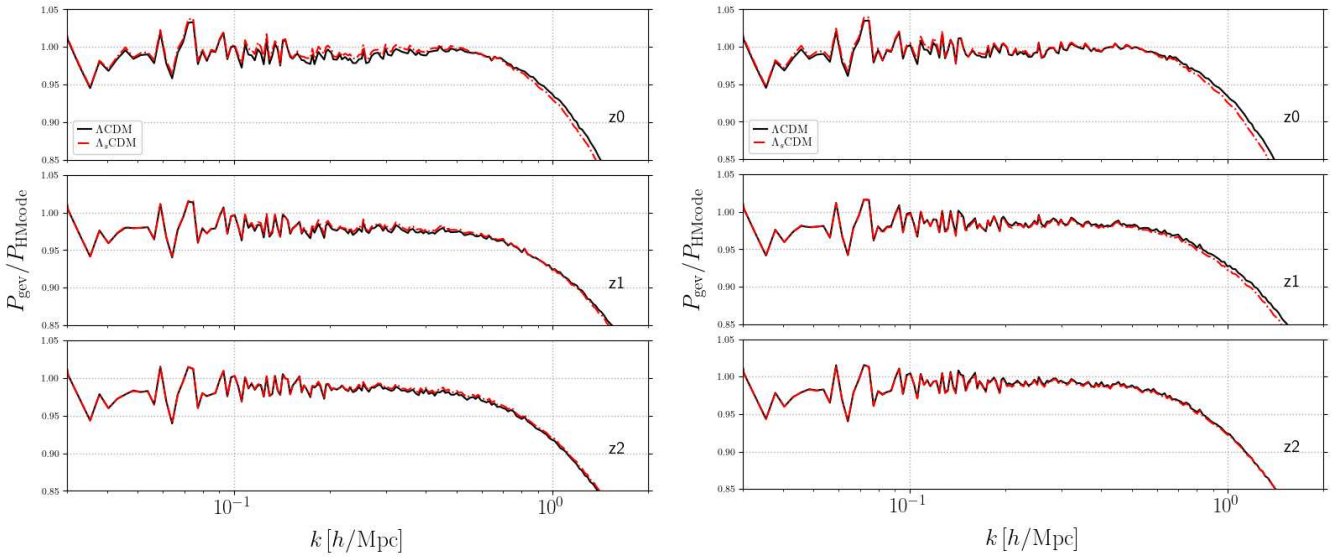

(a) *Planck*-only (b) full-dataset

FIG. 8. Ratios of the absolute cb-only power spectra from N-body simulations with `gevolution` to `CLASS` predictions including nonlinear corrections from `HMCode`, for (a) the *Planck*-only and (b) the full-dataset best-fit parameters, at $z = 2, 1$, and 0.

[1] N. Aghanim *et al.* (Planck), Planck 2018 results. VI. Cosmological parameters, Astron. Astrophys. **641**, A6 (2020), [Erratum: Astron.Astrophys. 652, C4 (2021)], 1807.06209.

[2] S. K. Choi *et al.* (ACT), The Atacama Cosmology Telescope: a measurement of the Cosmic Microwave Background power spectra at 98 and 150 GHz, JCAP **12**, 045, 2007.07289.

[3] E. Camphuis *et al.* (SPT-3G), SPT-3G D1: CMB temperature and polarization power spectra and cosmology

from 2019 and 2020 observations of the SPT-3G Main field (2025), 2506.20707.
[4] E. Abdalla *et al.*, Cosmology intertwined: A review of the particle physics, astrophysics, and cosmology associated with the cosmological tensions and anomalies, JHEAp **34**, 49 (2022), 2203.06142.
[5] L. Perivolaropoulos and F. Skara, Challenges for ΛCDM: An update, New Astron. Rev. **95**, 101659 (2022), 2105.05208.
[6] E. Di Valentino, Challenges of the Standard Cosmological Model, Universe **8**, 399 (2022).
[7] O. Akarsu, E. O. Colgáin, A. A. Sen, and M. M. Sheikh-Jabbari, ΛCDM Tensions: Localising Missing Physics through Consistency Checks, Universe **10**, 305 (2024), 2402.04767.
[8] E. Di Valentino *et al.* (CosmoVerse Network), The CosmoVerse White Paper: Addressing observational tensions in cosmology with systematics and fundamental physics, Phys. Dark Univ. **49**, 101965 (2025), 2504.01669.
[9] L. Verde, T. Treu, and A. G. Riess, Tensions between the Early and the Late Universe, Nature Astron. **3**, 891 (2019), 1907.10625.
[10] E. Di Valentino *et al.*, Snowmass2021 - Letter of interest cosmology intertwined II: The hubble constant tension, Astropart. Phys. **131**, 102605 (2021), 2008.11284.
[11] E. Di Valentino, O. Mena, S. Pan, L. Visinelli, W. Yang, A. Melchiorri, D. F. Mota, A. G. Riess, and J. Silk, In the realm of the Hubble tension—a review of solutions, Class. Quant. Grav. **38**, 153001 (2021), 2103.01183.
[12] N. Schöneberg, G. Franco Abellán, A. Pérez Sánchez, S. J. Witte, V. Poulin, and J. Lesgourgues, The H0 Olympics: A fair ranking of proposed models, Phys. Rept. **984**, 1 (2022), 2107.10291.
[13] P. Shah, P. Lemos, and O. Lahav, A buyer's guide to the Hubble constant, Astron. Astrophys. Rev. **29**, 9 (2021), 2109.01161.
[14] M. Kamionkowski and A. G. Riess, The Hubble Tension and Early Dark Energy, Ann. Rev. Nucl. Part. Sci. **73**, 153 (2023), 2211.04492.
[15] W. Giarè, CMB Anomalies and the Hubble Tension, in *The Hubble Constant Tension*, Springer Series in Astrophysics and Cosmology, edited by E. Di Valentino and D. Brout (Springer, Singapore, 2024) 2305.16919.
[16] J.-P. Hu and F.-Y. Wang, Hubble Tension: The Evidence of New Physics, Universe **9**, 94 (2023), 2302.05709.
[17] L. Verde, N. Schöneberg, and H. Gil-Marín, A tale of many H_0, Annu. Rev. Astron. Astrophys. **62**, 287 (2024), 2311.13305.
[18] E. Di Valentino and D. Brout, eds., *The Hubble Constant Tension*, Springer Series in Astrophysics and Cosmology (Springer, 2024).
[19] L. Perivolaropoulos, Hubble Tension or Distance Ladder Crisis?, Phys. Rev. D **110**, 123518 (2024), 2408.11031.
[20] W. L. Freedman, B. F. Madore, T. Hoyt, I. S. Jang, R. Beaton, M. G. Lee, A. Monson, J. Neeley, and J. Rich, Calibration of the Tip of the Red Giant Branch (TRGB), Astrophys. J. **891**, 57 (2020), 2002.01550.
[21] S. Birrer *et al.*, TDCOSMO - IV. Hierarchical time-delay cosmography – joint inference of the Hubble constant and galaxy density profiles, Astron. Astrophys. **643**, A165 (2020), 2007.02941.
[22] R. I. Anderson, N. W. Koblischke, and L. Eyer, Small-amplitude Red Giants Elucidate the Nature of the Tip of the Red Giant Branch as a Standard Candle, Astrophys. J. Lett. **963**, L43 (2024), 2303.04790.
[23] D. Scolnic, A. G. Riess, J. Wu, S. Li, G. S. Anand, R. Beaton, S. Casertano, R. I. Anderson, S. Dhawan, and X. Ke, CATS: The Hubble Constant from Standardized TRGB and Type Ia Supernova Measurements, Astrophys. J. Lett. **954**, L31 (2023), 2304.06693.
[24] D. O. Jones *et al.*, Cosmological Results from the RAISIN Survey: Using Type Ia Supernovae in the Near Infrared as a Novel Path to Measure the Dark Energy Equation of State, Astrophys. J. **933**, 172 (2022), 2201.07801.
[25] G. S. Anand, R. B. Tully, L. Rizzi, A. G. Riess, and W. Yuan, Comparing Tip of the Red Giant Branch Distance Scales: An Independent Reduction of the Carnegie-Chicago Hubble Program and the Value of the Hubble Constant, Astrophys. J. **932**, 15 (2022), 2108.00007.
[26] W. L. Freedman, Measurements of the Hubble Constant: Tensions in Perspective, Astrophys. J. **919**, 16 (2021), 2106.15656.
[27] S. A. Uddin *et al.*, Carnegie Supernova Project I and II: Measurements of H $_0$ Using Cepheid, Tip of the Red Giant Branch, and Surface Brightness Fluctuation Distance Calibration to Type Ia Supernovae*, Astrophys. J. **970**, 72 (2024), 2308.01875.
[28] C. D. Huang *et al.*, The Mira Distance to M101 and a 4% Measurement of H $_0$, Astrophys. J. **963**, 83 (2024), 2312.08423.
[29] S. Li, A. G. Riess, S. Casertano, G. S. Anand, D. M. Scolnic, W. Yuan, L. Breuval, and C. D. Huang, Reconnaissance with JWST of the J-region Asymptotic Giant Branch in Distance Ladder Galaxies: From Irregular Luminosity Functions to Approximation of the Hubble Constant, Astrophys. J. **966**, 20 (2024), 2401.04777.
[30] D. W. Pesce *et al.*, The Megamaser Cosmology Project. XIII. Combined Hubble constant constraints, Astrophys. J. Lett. **891**, L1 (2020), 2001.09213.
[31] E. Kourkchi, R. B. Tully, G. S. Anand, H. M. Courtois, A. Dupuy, J. D. Neill, L. Rizzi, and M. Seibert, Cosmicflows-4: The Calibration of Optical and Infrared Tully–Fisher Relations, Astrophys. J. **896**, 3 (2020), 2004.14499.
[32] J. Schombert, S. McGaugh, and F. Lelli, Using the Baryonic Tully–Fisher Relation to Measure H o, Astron. J. **160**, 71 (2020), 2006.08615.
[33] J. P. Blakeslee, J. B. Jensen, C.-P. Ma, P. A. Milne, and J. E. Greene, The Hubble Constant from Infrared Surface Brightness Fluctuation Distances, Astrophys. J. **911**, 65 (2021), 2101.02221.
[34] T. de Jaeger, L. Galbany, A. G. Riess, B. E. Stahl, B. J. Shappee, A. V. Filippenko, and W. Zheng, A 5 per cent measurement of the Hubble–Lemaître constant from Type II supernovae, Mon. Not. Roy. Astron. Soc. **514**, 4620 (2022), 2203.08974.
[35] Y. S. Murakami, A. G. Riess, B. E. Stahl, W. D. Kenworthy, D.-M. A. Pluck, A. Macoretta, D. Brout, D. O. Jones, D. M. Scolnic, and A. V. Filippenko, Leveraging SN Ia spectroscopic similarity to improve the measurement of H $_0$, JCAP **11**, 046, 2306.00070.
[36] L. Breuval, A. G. Riess, S. Casertano, W. Yuan, L. M. Macri, M. Romaniello, Y. S. Murakami, D. Scolnic, G. S. Anand, and I. Soszyński, Small Magellanic Cloud Cepheids Observed with the Hubble Space Telescope Provide a New Anchor for the SH0ES Distance Ladder, Astrophys. J. **973**, 30 (2024), 2404.08038.
[37] W. L. Freedman, B. F. Madore, T. J. Hoyt, I. S. Jang,

A. J. Lee, and K. A. Owens, Status Report on the Chicago-Carnegie Hubble Program (CCHP): Measurement of the Hubble Constant Using the Hubble and James Webb Space Telescopes, Astrophys. J. **985**, 203 (2025), 2408.06153.

[38] A. G. Riess *et al.*, JWST Validates HST Distance Measurements: Selection of Supernova Subsample Explains Differences in JWST Estimates of Local H $_0$, Astrophys. J. **977**, 120 (2024), 2408.11770.

[39] C. Vogl *et al.*, No rungs attached: A distance-ladder free determination of the Hubble constant through type II supernova spectral modelling, Astron. Astrophys. **702**, A41 (2025), 2411.04968.

[40] D. Scolnic *et al.*, The Hubble Tension in Our Own Backyard: DESI and the Nearness of the Coma Cluster, Astrophys. J. Lett. **979**, L9 (2025), 2409.14546.

[41] K. Said *et al.*, DESI Peculiar Velocity Survey – Fundamental Plane, Mon. Not. Roy. Astron. Soc. **539**, 3627 (2025), 2408.13842.

[42] P. Boubel, M. Colless, K. Said, and L. Staveley-Smith, An improved Tully–Fisher estimate of H0, Mon. Not. Roy. Astron. Soc. **533**, 1550 (2024), 2408.03660.

[43] D. Scolnic, P. Boubel, J. Byrne, A. G. Riess, and G. S. Anand, Calibrating the Tully-Fisher Relation to Measure the Hubble Constant (2024), 2412.08449.

[44] S. Li, A. G. Riess, D. Scolnic, S. Casertano, and G. S. Anand, JAGB 2.0: Improved Constraints on the J-region Asymptotic Giant Branch–based Hubble Constant from an Expanded Sample of JWST Observations, Astrophys. J. **988**, 97 (2025), 2502.05259.

[45] J. B. Jensen, J. P. Blakeslee, M. Cantiello, M. Cowles, G. S. Anand, R. B. Tully, E. Kourkchi, and G. Raimondo, The TRGB-SBF Project. III. Refining the HST Surface Brightness Fluctuation Distance Scale Calibration with JWST, Astrophys. J. **987**, 87 (2025), 2502.15935.

[46] A. G. Riess *et al.*, The Perfect Host: JWST Cepheid Observations in a Background-Free SN Ia Host Confirm No Bias in Hubble-Constant Measurements (2025), 2509.01667.

[47] M. J. B. Newman *et al.*, Tip of the Red Giant Branch Distances to NGC 1316, NGC 1380, NGC 1404, & NGC 4457: A Pilot Study of a Parallel Distance Ladder Using Type Ia Supernovae in Early-Type Host Galaxies (2025), 2508.20023.

[48] R. Stiskalek, H. Desmond, E. Tsaprazi, A. Heavens, G. Lavaux, S. McAlpine, and J. Jasche, 1.8 per cent measurement of H_0 from Cepheids alone, Mon. Not. R. Astron. Soc. **546**, staf2260 (2026), 2509.09665.

[49] S. Casertano *et al.* (H0DN), The Local Distance Network: a community consensus report on the measurement of the Hubble constant at 1% precision (2025), 2510.23823.

[50] E. Di Valentino *et al.*, Cosmology Intertwined III: $f\sigma_8$ and S_8, Astropart. Phys. **131**, 102604 (2021), 2008.11285.

[51] E. Di Valentino and S. Bridle, Exploring the Tension between Current Cosmic Microwave Background and Cosmic Shear Data, Symmetry **10**, 585 (2018).

[52] R. C. Nunes and S. Vagnozzi, Arbitrating the S8 discrepancy with growth rate measurements from redshift-space distortions, Mon. Not. Roy. Astron. Soc. **505**, 5427 (2021), 2106.01208.

[53] A. Amon *et al.* (DES), Dark Energy Survey Year 3 results: Cosmology from cosmic shear and robustness to data calibration, Phys. Rev. D **105**, 023514 (2022), 2105.13543.

[54] L. F. Secco *et al.* (DES), Dark Energy Survey Year 3 results: Cosmology from cosmic shear and robustness to modeling uncertainty, Phys. Rev. D **105**, 023515 (2022), 2105.13544.

[55] M. Asgari *et al.* (KiDS), KiDS-1000 Cosmology: Cosmic shear constraints and comparison between two point statistics, Astron. Astrophys. **645**, A104 (2021), 2007.15633.

[56] M. Asgari *et al.*, KiDS+VIKING-450 and DES-Y1 combined: Mitigating baryon feedback uncertainty with COSEBIs, Astron. Astrophys. **634**, A127 (2020), 1910.05336.

[57] S. Joudaki *et al.*, KiDS+VIKING-450 and DES-Y1 combined: Cosmology with cosmic shear, Astron. Astrophys. **638**, L1 (2020), 1906.09262.

[58] G. D'Amico, J. Gleyzes, N. Kokron, K. Markovic, L. Senatore, P. Zhang, F. Beutler, and H. Gil-Marín, The Cosmological Analysis of the SDSS/BOSS data from the Effective Field Theory of Large-Scale Structure, JCAP **05**, 005, 1909.05271.

[59] T. M. C. Abbott *et al.* (Kilo-Degree Survey, DES), DES Y3 + KiDS-1000: Consistent cosmology combining cosmic shear surveys, Open J. Astrophys. **6**, 2305.17173 (2023), 2305.17173.

[60] T. Tröster *et al.*, Cosmology from large-scale structure: Constraining ΛCDM with BOSS, Astron. Astrophys. **633**, L10 (2020), 1909.11006.

[61] C. Heymans *et al.*, KiDS-1000 Cosmology: Multi-probe weak gravitational lensing and spectroscopic galaxy clustering constraints, Astron. Astrophys. **646**, A140 (2021), 2007.15632.

[62] R. Dalal *et al.*, Hyper Suprime-Cam Year 3 results: Cosmology from cosmic shear power spectra, Phys. Rev. D **108**, 123519 (2023), 2304.00701.

[63] S. Chen *et al.*, Not all lensing is low: An analysis of DESI×DES using the Lagrangian Effective Theory of LSS (2024), 2407.04795.

[64] J. Kim *et al.* (ACT, DESI), The Atacama Cosmology Telescope DR6 and DESI: Structure formation over cosmic time with a measurement of the cross-correlation of CMB Lensing and Luminous Red Galaxies, JCAP **12**, 022, 2407.04606.

[65] L. Faga *et al.* (DES), Dark Energy Survey Year 3 Results: Cosmology from galaxy clustering and galaxy-galaxy lensing in harmonic space, Mon. Not. R. Astron. Soc. **536**, 1586 (2024), 2406.12675.

[66] J. Harnois-Deraps *et al.*, KiDS-1000 and DES-Y1 combined: Cosmology from peak count statistics (2024), 2405.10312.

[67] A. Dvornik *et al.*, KiDS-1000: Combined halo-model cosmology constraints from galaxy abundance, galaxy clustering and galaxy-galaxy lensing, Astron. Astrophys. **675**, A189 (2023), [Erratum: Astron. Astrophys. 688, C3 (2024)], 2210.03110.

[68] T. M. C. Abbott *et al.* (DES), Dark Energy Survey Year 3 results: Cosmological constraints from galaxy clustering and weak lensing, Phys. Rev. D **105**, 023520 (2022), 2105.13549.

[69] A. H. Wright *et al.*, KiDS-Legacy: Cosmological constraints from cosmic shear with the complete Kilo-Degree Survey, Astron. Astrophys. **703**, A158 (2025), 2503.19441.

[70] S. A. Adil, Ö. Akarsu, M. Malekjani, E. Ó. Colgáin,

S. Pourojaghi, A. A. Sen, and M. M. Sheikh-Jabbari, S8 increases with effective redshift in ΛCDM cosmology, Mon. Not. Roy. Astron. Soc. **528**, L20 (2023), 2303.06928.

[71] Ö. Akarsu, E. Ó. Colgáin, A. A. Sen, and M. M. Sheikh-Jabbari, Further support for S_8 increasing with effective redshift, Mon. Not. Roy. Astron. Soc. **542**, L36 (2025), 2410.23134.

[72] V. Poulin, T. L. Smith, T. Karwal, and M. Kamionkowski, Early Dark Energy Can Resolve The Hubble Tension, Phys. Rev. Lett. **122**, 221301 (2019), 1811.04083.

[73] T. Karwal and M. Kamionkowski, Dark energy at early times, the Hubble parameter, and the string axiverse, Phys. Rev. D **94**, 103523 (2016), 1608.01309.

[74] J. C. Hill, E. McDonough, M. W. Toomey, and S. Alexander, Early dark energy does not restore cosmological concordance, Phys. Rev. D **102**, 043507 (2020), 2003.07355.

[75] M. M. Ivanov, E. McDonough, J. C. Hill, M. Simonović, M. W. Toomey, S. Alexander, and M. Zaldarriaga, Constraining Early Dark Energy with Large-Scale Structure, Phys. Rev. D **102**, 103502 (2020), 2006.11235.

[76] J. Sakstein and M. Trodden, Early Dark Energy from Massive Neutrinos as a Natural Resolution of the Hubble Tension, Phys. Rev. Lett. **124**, 161301 (2020), 1911.11760.

[77] F. Niedermann and M. S. Sloth, New early dark energy, Phys. Rev. D **103**, L041303 (2021), 1910.10739.

[78] F. Niedermann and M. S. Sloth, Resolving the Hubble tension with new early dark energy, Phys. Rev. D **102**, 063527 (2020), 2006.06686.

[79] V. Poulin, T. L. Smith, and T. Karwal, The Ups and Downs of Early Dark Energy solutions to the Hubble tension: A review of models, hints and constraints circa 2023, Phys. Dark Univ. **42**, 101348 (2023), 2302.09032.

[80] A. Smith, P. Brax, C. van de Bruck, C. P. Burgess, and A.-C. Davis, Screened Axio-dilaton Cosmology: Novel Forms of Early Dark Energy, Eur. Phys. J. C **85**, 1062 (2025), 2505.05450.

[81] V. Poulin, T. L. Smith, R. Calderón, and T. Simon, Impact of ACT DR6 and DESI DR2 for Early Dark Energy and the Hubble tension (2025), 2505.08051.

[82] A. R. Khalife *et al.* (SPT-3G), SPT-3G D1: Axion Early Dark Energy with CMB experiments and DESI (2025), 2507.23355.

[83] E. Di Valentino, A. Melchiorri, and O. Mena, Can interacting dark energy solve the H_0 tension?, Phys. Rev. D **96**, 043503 (2017), 1704.08342.

[84] E. Di Valentino, A. Melchiorri, O. Mena, and S. Vagnozzi, Interacting dark energy in the early 2020s: A promising solution to the H_0 and cosmic shear tensions, Phys. Dark Univ. **30**, 100666 (2020), 1908.04281.

[85] W. Yang, S. Pan, E. Di Valentino, R. C. Nunes, S. Vagnozzi, and D. F. Mota, Tale of stable interacting dark energy, observational signatures, and the H_0 tension, JCAP **09**, 019, 1805.08252.

[86] W. Yang, A. Mukherjee, E. Di Valentino, and S. Pan, Interacting dark energy with time varying equation of state and the H_0 tension, Phys. Rev. D **98**, 123527 (2018), 1809.06883.

[87] R. C. Nunes, S. Pan, and E. N. Saridakis, New constraints on interacting dark energy from cosmic chronometers, Phys. Rev. D **94**, 023508 (2016), 1605.01712.

[88] W. Giarè, M. A. Sabogal, R. C. Nunes, and E. Di Valentino, Interacting Dark Energy after DESI Baryon Acoustic Oscillation measurements, Phys. Rev. Lett. **133**, 251003 (2024), 2404.15232.

[89] C. Caprini and N. Tamanini, Constraining early and interacting dark energy with gravitational wave standard sirens: the potential of the eLISA mission, JCAP **10**, 006, 1607.08755.

[90] W. Yang, S. Pan, E. Di Valentino, O. Mena, and A. Melchiorri, 2021-H0 odyssey: closed, phantom and interacting dark energy cosmologies, JCAP **10**, 008, 2101.03129.

[91] W. Yang, S. Pan, and D. F. Mota, Novel approach toward the large-scale stable interacting dark-energy models and their astronomical bounds, Phys. Rev. D **96**, 123508 (2017), 1709.00006.

[92] S. Pan, G. S. Sharov, and W. Yang, Field theoretic interpretations of interacting dark energy scenarios and recent observations, Phys. Rev. D **101**, 103533 (2020), 2001.03120.

[93] L. A. Escamilla, O. Akarsu, E. Di Valentino, and J. A. Vazquez, Model-independent reconstruction of the interacting dark energy kernel: Binned and Gaussian process, JCAP **11**, 051, 2305.16290.

[94] A. Bernui, E. Di Valentino, W. Giarè, S. Kumar, and R. C. Nunes, Exploring the H0 tension and the evidence for dark sector interactions from 2D BAO measurements, Phys. Rev. D **107**, 103531 (2023), 2301.06097.

[95] L.-Y. Gao, Z.-W. Zhao, S.-S. Xue, and X. Zhang, Relieving the H 0 tension with a new interacting dark energy model, JCAP **07**, 005, 2101.10714.

[96] T.-N. Li, P.-J. Wu, G.-H. Du, S.-J. Jin, H.-L. Li, J.-F. Zhang, and X. Zhang, Constraints on interacting dark energy models from the DESI BAO and DES supernovae data, Astrophys. J. **976**, 1 (2024), 2407.14934.

[97] A. A. Costa, R. C. G. Landim, B. Wang, and E. Abdalla, Interacting Dark Energy: Possible Explanation for 21-cm Absorption at Cosmic Dawn, Eur. Phys. J. C **78**, 746 (2018), 1803.06944.

[98] E. Di Valentino, A. Melchiorri, O. Mena, S. Pan, and W. Yang, Interacting Dark Energy in a closed universe, Mon. Not. Roy. Astron. Soc. **502**, L23 (2021), 2011.00283.

[99] R. von Marttens, L. Casarini, D. F. Mota, and W. Zimdahl, Cosmological constraints on parametrized interacting dark energy, Phys. Dark Univ. **23**, 100248 (2019), 1807.11380.

[100] E. Silva, M. A. Sabogal, M. Scherer, R. C. Nunes, E. Di Valentino, and S. Kumar, New constraints on interacting dark energy from DESI DR2 BAO observations, Phys. Rev. D **111**, 123511 (2025), 2503.23225.

[101] W. Yang, S. Zhang, O. Mena, S. Pan, and E. Di Valentino, Dark Energy Is Not That Into You: Variable Couplings after DESI DR2 BAO (2025), 2508.19109.

[102] M. van der Westhuizen, A. Abebe, and E. Di Valentino, III. Interacting Dark Energy: Summary of Models, Pathologies, and Constraints, Phys. Dark Univ. **50**, 102121 (2025), 2509.04496.

[103] A. G. Adame *et al.* (DESI), DESI 2024 VI: Cosmological Constraints from the Measurements of Baryon Acoustic Oscillations, JCAP **02**, 021, 2404.03002.

[104] M. Abdul Karim *et al.* (DESI), DESI DR2 Results II: Measurements of Baryon Acoustic Oscillations and Cosmological Constraints, Phys. Rev. D **112**, 083515 (2025), 2503.14738.

[105] W. Giarè, M. Najafi, S. Pan, E. Di Valentino, and J. T. Firouzjaee, Robust preference for Dynamical Dark Energy in DESI BAO and SN measurements, JCAP **10**, 035, 2407.16689.

[106] I. D. Gialamas, G. Hütsi, K. Kannike, A. Racioppi, M. Raidal, M. Vasar, and H. Veermäe, Interpreting DESI 2024 BAO: late-time dynamical dark energy or a local effect?, Phys. Rev. D **111**, 043540 (2025), 2406.07533.

[107] S. Roy Choudhury and T. Okumura, Updated Cosmological Constraints in Extended Parameter Space with Planck PR4, DESI Baryon Acoustic Oscillations, and Supernovae: Dynamical Dark Energy, Neutrino Masses, Lensing Anomaly, and the Hubble Tension, Astrophys. J. Lett. **976**, L11 (2024), 2409.13022.

[108] B. R. Dinda, A new diagnostic for the null test of dynamical dark energy in light of DESI 2024 and other BAO data, JCAP **09**, 062, 2405.06618.

[109] W. Giarè, Dynamical dark energy beyond Planck? Constraints from multiple CMB probes, DESI BAO, and type-Ia supernovae, Phys. Rev. D **112**, 023508 (2025), 2409.17074.

[110] S. Roy Choudhury, Cosmology in Extended Parameter Space with DESI DR2 BAO: A $2\sigma+$ Detection of Nonzero Neutrino Masses with an Update on Dynamical Dark Energy and Lensing Anomaly, Astrophys. J. Lett. **986**, L31 (2025), 2504.15340.

[111] S. Roy Choudhury, T. Okumura, and K. Umetsu, Cosmological Constraints on Nonphantom Dynamical Dark Energy with DESI Data Release 2 Baryon Acoustic Oscillations: A $3\sigma+$ Lensing Anomaly, Astrophys. J. Lett. **994**, L26 (2025), 2509.26144.

[112] M. Scherer, M. A. Sabogal, R. C. Nunes, and A. De Felice, Challenging the ΛCDM model: 5σ evidence for a dynamical dark energy late-time transition, Phys. Rev. D **112**, 043513 (2025), 2504.20664.

[113] Y.-H. Pang, X. Zhang, and Q.-G. Huang, The Impact of the Hubble Tension on the Evidence for Dynamical Dark Energy, Sci. China Phys. Mech. Astron. **68**, 280410 (2025), 2503.21600.

[114] N. Roy, Dynamical dark energy in the light of DESI 2024 data, Phys. Dark Univ. **48**, 101912 (2025), 2406.00634.

[115] A. N. Ormondroyd, W. J. Handley, M. P. Hobson, and A. N. Lasenby, Comparison of dynamical dark energy with ΛCDM in light of DESI DR2 (2025), 2503.17342.

[116] C. Li, J. Wang, D. Zhang, E. N. Saridakis, and Y.-F. Cai, Quantum gravity meets DESI: dynamical dark energy in light of the trans-Planckian censorship conjecture, JCAP **08**, 041, 2504.07791.

[117] M. Cortês and A. R. Liddle, Interpreting DESI's evidence for evolving dark energy, JCAP **12**, 007, 2404.08056.

[118] M. Najafi, S. Pan, E. Di Valentino, and J. T. Firouzjaee, Dynamical dark energy confronted with multiple CMB missions, Phys. Dark Univ. **45**, 101539 (2024), 2407.14939.

[119] H. Wang and Y.-S. Piao, Dark energy in light of DESI DR1 and Hubble tension, Phys. Lett. B **873**, 140180 (2026), 2404.18579.

[120] W. Giarè, Dynamical dark energy beyond Planck? Constraints from multiple CMB probes, DESI BAO, and type-Ia supernovae, Phys. Rev. D **112**, 023508 (2025), 2409.17074.

[121] W. Giarè, T. Mahassen, E. Di Valentino, and S. Pan, An overview of what current data can (and cannot yet) say about evolving dark energy, Phys. Dark Univ. **48**, 101906 (2025), 2502.10264.

[122] D. A. Kessler, L. A. Escamilla, S. Pan, and E. Di Valentino, One-parameter dynamical dark energy: Hints for oscillations (2025), 2504.00776.

[123] E. M. Teixeira, W. Giarè, N. B. Hogg, T. Montandon, A. Poudou, and V. Poulin, Implications of distance duality violation for the H_0 tension and evolving dark energy (2025), 2504.10464.

[124] E. Specogna, S. A. Adil, E. Ozulker, E. Di Valentino, R. C. Nunes, O. Akarsu, and A. A. Sen, Updated Constraints on Omnipotent Dark Energy: A Comprehensive Analysis with CMB and BAO Data (2025), 2504.17859.

[125] M. A. Sabogal and R. C. Nunes, Robust Evidence for Dynamical Dark Energy from DESI Galaxy-CMB Lensing Cross-Correlation and Geometric Probes, JCAP **09**, 084, 2505.24465.

[126] H. Cheng, E. Di Valentino, L. A. Escamilla, A. A. Sen, and L. Visinelli, Pressure Parametrization of Dark Energy: First and Second-Order Constraints with Latest Cosmological Data, JCAP **09**, 031, 2505.02932.

[127] L. Herold and T. Karwal, Bayesian and frequentist perspectives agree on dynamical dark energy (2025), 2506.12004.

[128] H. Cheng, E. Di Valentino, and L. Visinelli, Cosmic Strings as Dynamical Dark Energy: Novel Constraints (2025), 2505.22066.

[129] E. Özülker, E. Di Valentino, and W. Giarè, Dark Energy Crosses the Line: Quantifying and Testing the Evidence for Phantom Crossing (2025), 2506.19053.

[130] D. H. Lee, W. Yang, E. Di Valentino, S. Pan, and C. van de Bruck, The Shape of Dark Energy: Constraining Its Evolution with a General Parametrization (2025), 2507.11432.

[131] E. Silva and R. C. Nunes, Testing Signatures of Phantom Crossing through Full-Shape Galaxy Clustering Analysis, JCAP **11**, 078, 2507.13989.

[132] E. Fazzari, W. Giarè, and E. Di Valentino, Cosmographic Footprints of Dynamical Dark Energy, Astrophys. J. Lett. **996**, L5 (2026), 2509.16196.

[133] O. Akarsu, J. D. Barrow, L. A. Escamilla, and J. A. Vazquez, Graduated dark energy: Observational hints of a spontaneous sign switch in the cosmological constant, Phys. Rev. D **101**, 063528 (2020), 1912.08751.

[134] O. Akarsu, S. Kumar, E. Özülker, and J. A. Vazquez, Relaxing cosmological tensions with a sign switching cosmological constant, Phys. Rev. D **104**, 123512 (2021), 2108.09239.

[135] O. Akarsu, S. Kumar, E. Özülker, J. A. Vazquez, and A. Yadav, Relaxing cosmological tensions with a sign switching cosmological constant: Improved results with Planck, BAO, and Pantheon data, Phys. Rev. D **108**, 023513 (2023), 2211.05742.

[136] O. Akarsu, E. Di Valentino, S. Kumar, R. C. Nunes, J. A. Vazquez, and A. Yadav, Λ_sCDM model: A promising scenario for alleviation of cosmological tensions (2023), 2307.10899.

[137] Ö. Akarsu, A. De Felice, E. Di Valentino, S. Kumar, R. C. Nunes, E. Özülker, J. A. Vazquez, and A. Yadav, Cosmological constraints on ΛsCDM scenario in a type II minimally modified gravity, Phys. Rev. D **110**, 103527 (2024), 2406.07526.

[138] A. Yadav, S. Kumar, C. Kibris, and O. Akarsu, Λ_sCDM cosmology: alleviating major cosmological tensions by predicting standard neutrino properties, JCAP **01**, 042,

2406.18496.
[139] L. A. Escamilla, Ö. Akarsu, E. Di Valentino, E. Özülker, and J. A. Vazquez, Exploring the Growth-Index (γ) Tension with Λ_sCDM (2025), 2503.12945.
[140] E. A. Paraskevas, A. Cam, L. Perivolaropoulos, and O. Akarsu, Transition dynamics in the ΛsCDM model: Implications for bound cosmic structures, Phys. Rev. D **109**, 103522 (2024), 2402.05908.
[141] Ö. Akarsu, A. Çam, E. A. Paraskevas, and L. Perivolaropoulos, Linear matter density perturbations in the Λ_sCDM model: Examining growth dynamics and addressing the S $_8$ tension, JCAP **08**, 089, 2502.20384.
[142] V. Sahni and Y. Shtanov, Brane world models of dark energy, JCAP **11**, 014, astro-ph/0202346.
[143] J. A. Vazquez, S. Hee, M. P. Hobson, A. N. Lasenby, M. Ibison, and M. Bridges, Observational constraints on conformal time symmetry, missing matter and double dark energy, JCAP **07**, 062, 1208.2542.
[144] T. Delubac *et al.* (BOSS), Baryon acoustic oscillations in the Lyα forest of BOSS DR11 quasars, Astron. Astrophys. **574**, A59 (2015), 1404.1801.
[145] V. Sahni, A. Shafieloo, and A. A. Starobinsky, Model independent evidence for dark energy evolution from Baryon Acoustic Oscillations, Astrophys. J. Lett. **793**, L40 (2014), 1406.2209.
[146] E. Aubourg *et al.* (BOSS), Cosmological implications of baryon acoustic oscillation measurements, Phys. Rev. D **92**, 123516 (2015), 1411.1074.
[147] E. Di Valentino, E. V. Linder, and A. Melchiorri, Vacuum phase transition solves the H_0 tension, Phys. Rev. D **97**, 043528 (2018), 1710.02153.
[148] E. Mörtsell and S. Dhawan, Does the Hubble constant tension call for new physics?, JCAP **09**, 025, 1801.07260.
[149] V. Poulin, K. K. Boddy, S. Bird, and M. Kamionkowski, Implications of an extended dark energy cosmology with massive neutrinos for cosmological tensions, Phys. Rev. D **97**, 123504 (2018), 1803.02474.
[150] S. Capozziello, Ruchika, and A. A. Sen, Model independent constraints on dark energy evolution from low-redshift observations, Mon. Not. Roy. Astron. Soc. **484**, 4484 (2019), 1806.03943.
[151] Y. Wang, L. Pogosian, G.-B. Zhao, and A. Zucca, Evolution of dark energy reconstructed from the latest observations, Astrophys. J. Lett. **869**, L8 (2018), 1807.03772.
[152] A. Banihashemi, N. Khosravi, and A. H. Shirazi, Phase transition in the dark sector as a proposal to lessen cosmological tensions, Phys. Rev. D **101**, 123521 (2020), 1808.02472.
[153] K. Dutta, Ruchika, A. Roy, A. A. Sen, and M. M. Sheikh-Jabbari, Beyond ΛCDM with low and high redshift data: implications for dark energy, Gen. Rel. Grav. **52**, 15 (2020), 1808.06623.
[154] A. Banihashemi, N. Khosravi, and A. H. Shirazi, Ginzburg-Landau Theory of Dark Energy: A Framework to Study Both Temporal and Spatial Cosmological Tensions Simultaneously, Phys. Rev. D **99**, 083509 (2019), 1810.11007.
[155] Ö. Akarsu, J. D. Barrow, C. V. R. Board, N. M. Uzun, and J. A. Vazquez, Screening Λ in a new modified gravity model, Eur. Phys. J. C **79**, 846 (2019), 1903.11519.
[156] X. Li and A. Shafieloo, A Simple Phenomenological Emergent Dark Energy Model can Resolve the Hubble Tension, Astrophys. J. Lett. **883**, L3 (2019), 1906.08275.
[157] L. Visinelli, S. Vagnozzi, and U. Danielsson, Revisiting a negative cosmological constant from low-redshift data, Symmetry **11**, 1035 (2019), 1907.07953.
[158] G. Ye and Y.-S. Piao, Is the Hubble tension a hint of AdS phase around recombination?, Phys. Rev. D **101**, 083507 (2020), 2001.02451.
[159] A. Perez, D. Sudarsky, and E. Wilson-Ewing, Resolving the H_0 tension with diffusion, Gen. Rel. Grav. **53**, 7 (2021), 2001.07536.
[160] Ö. Akarsu, N. Katırcı, S. Kumar, R. C. Nunes, B. Öztürk, and S. Sharma, Rastall gravity extension of the standard ΛCDM model: theoretical features and observational constraints, Eur. Phys. J. C **80**, 1050 (2020), 2004.04074.
[161] Ruchika, S. A. Adil, K. Dutta, A. Mukherjee, and A. A. Sen, Observational constraints on axion(s) dark energy with a cosmological constant, Phys. Dark Univ. **40**, 101199 (2023), 2005.08813.
[162] E. Di Valentino, A. Mukherjee, and A. A. Sen, Dark Energy with Phantom Crossing and the H_0 Tension, Entropy **23**, 404 (2021), 2005.12587.
[163] R. Calderón, R. Gannouji, B. L'Huillier, and D. Polarski, Negative cosmological constant in the dark sector?, Phys. Rev. D **103**, 023526 (2021), 2008.10237.
[164] G. Ye and Y.-S. Piao, T_0 censorship of early dark energy and AdS vacua, Phys. Rev. D **102**, 083523 (2020), 2008.10832.
[165] A. De Felice, S. Mukohyama, and M. C. Pookkillath, Addressing H_0 tension by means of VCDM, Phys. Lett. B **816**, 136201 (2021), [Erratum: Phys.Lett.B 818, 136364 (2021)], 2009.08718.
[166] A. Paliathanasis and G. Leon, Dynamics of a two scalar field cosmological model with phantom terms, Class. Quant. Grav. **38**, 075013 (2021), 2009.12874.
[167] A. Bonilla, S. Kumar, and R. C. Nunes, Measurements of H_0 and reconstruction of the dark energy properties from a model-independent joint analysis, Eur. Phys. J. C **81**, 127 (2021), 2011.07140.
[168] G. Acquaviva, O. Akarsu, N. Katirci, and J. A. Vazquez, Simple-graduated dark energy and spatial curvature, Phys. Rev. D **104**, 023505 (2021), 2104.02623.
[169] S. Bag, V. Sahni, A. Shafieloo, and Y. Shtanov, Phantom Braneworld and the Hubble Tension, Astrophys. J. **923**, 212 (2021), 2107.03271.
[170] R. C. Bernardo, D. Grandón, J. Said Levi, and V. H. Cárdenas, Parametric and nonparametric methods hint dark energy evolution, Phys. Dark Univ. **36**, 101017 (2022), 2111.08289.
[171] L. A. Escamilla and J. A. Vazquez, Model selection applied to reconstructions of the Dark Energy, Eur. Phys. J. C **83**, 251 (2023), 2111.10457.
[172] A. A. Sen, S. A. Adil, and S. Sen, Do cosmological observations allow a negative Λ?, Mon. Not. Roy. Astron. Soc. **518**, 1098 (2022), 2112.10641.
[173] E. Ozulker, Is the dark energy equation of state parameter singular?, Phys. Rev. D **106**, 063509 (2022), 2203.04167.
[174] S. Di Gennaro and Y. C. Ong, Sign Switching Dark Energy from a Running Barrow Entropy, Universe **8**, 541 (2022), 2205.09311.
[175] O. Akarsu, E. O. Colgain, E. Özulker, S. Thakur, and L. Yin, Inevitable manifestation of wiggles in the expansion of the late Universe, Phys. Rev. D **107**, 123526 (2023), 2207.10609.
[176] H. Moshafi, H. Firouzjahi, and A. Talebian, Multiple Transitions in Vacuum Dark Energy and H $_0$ Tension,

Astrophys. J. **940**, 121 (2022), 2208.05583.
[177] R. C. Bernardo, D. Grandón, J. Levi Said, and V. H. Cárdenas, Dark energy by natural evolution: Constraining dark energy using Approximate Bayesian Computation, Phys. Dark Univ. **40**, 101213 (2023), 2211.05482.
[178] A. van de Venn, D. Vasak, J. Kirsch, and J. Struckmeier, Torsional dark energy in quadratic gauge gravity, Eur. Phys. J. C **83**, 288 (2023), 2211.11868.
[179] Y. C. Ong, An Effective Sign Switching Dark Energy: Lotka–Volterra Model of Two Interacting Fluids, Universe **9**, 437 (2023), 2212.04429.
[180] Y. Tiwari, B. Ghosh, and R. K. Jain, Towards a possible solution to the Hubble tension with Horndeski gravity, Eur. Phys. J. C **84**, 220 (2024), 2301.09382.
[181] M. Malekjani, R. M. Conville, E. Ó. Colgáin, S. Pourojaghi, and M. M. Sheikh-Jabbari, On redshift evolution and negative dark energy density in Pantheon + Supernovae, Eur. Phys. J. C **84**, 317 (2024), 2301.12725.
[182] J. A. Vázquez, D. Tamayo, G. Garcia-Arroyo, I. Gómez-Vargas, I. Quiros, and A. A. Sen, Coupled multiscalar field dark energy, Phys. Rev. D **109**, 023511 (2024), 2305.11396.
[183] S. A. Adil, O. Akarsu, E. Di Valentino, R. C. Nunes, E. Özülker, A. A. Sen, and E. Specogna, Omnipotent dark energy: A phenomenological answer to the Hubble tension, Phys. Rev. D **109**, 023527 (2024), 2306.08046.
[184] B. Alexandre, S. Gielen, and J. Magueijo, Overall signature of the metric and the cosmological constant, JCAP **02**, 036, 2306.11502.
[185] S. A. Adil, U. Mukhopadhyay, A. A. Sen, and S. Vagnozzi, Dark energy in light of the early JWST observations: case for a negative cosmological constant?, JCAP **10**, 072, 2307.12763.
[186] E. A. Paraskevas and L. Perivolaropoulos, The density of virialized clusters as a probe of dark energy, Mon. Not. Roy. Astron. Soc. **531**, 1021 (2024), 2308.07046.
[187] A. Gómez-Valent, A. Favale, M. Migliaccio, and A. A. Sen, Late-time phenomenology required to solve the H0 tension in view of the cosmic ladders and the anisotropic and angular BAO datasets, Phys. Rev. D **109**, 023525 (2024), 2309.07795.
[188] R. Y. Wen, L. T. Hergt, N. Afshordi, and D. Scott, A cosmic glitch in gravity, JCAP **03**, 045, 2311.03028.
[189] R. Medel-Esquivel, I. Gómez-Vargas, A. A. M. Sánchez, R. García-Salcedo, and J. Alberto Vázquez, Cosmological Parameter Estimation with Genetic Algorithms, Universe **10**, 11 (2024), 2311.05699.
[190] A. De Felice, S. Kumar, S. Mukohyama, and R. C. Nunes, Observational bounds on extended minimal theories of massive gravity: new limits on the graviton mass, JCAP **04**, 013, 2311.10530.
[191] L. A. Anchordoqui, I. Antoniadis, and D. Lust, Anti-de Sitter → de Sitter transition driven by Casimir forces and mitigating tensions in cosmological parameters, Phys. Lett. B **855**, 138775 (2024), 2312.12352.
[192] N. Menci, S. A. Adil, U. Mukhopadhyay, A. A. Sen, and S. Vagnozzi, Negative cosmological constant in the dark energy sector: tests from JWST photometric and spectroscopic observations of high-redshift galaxies, JCAP **07**, 072, 2401.12659.
[193] L. A. Anchordoqui, I. Antoniadis, D. Lust, N. T. Noble, and J. F. Soriano, From infinite to infinitesimal: Using the Universe as a dataset to probe Casimir corrections to the vacuum energy from fields inhabiting the dark dimension, Phys. Dark Univ. **46**, 101715 (2024), 2404.17334.
[194] O. Akarsu, A. De Felice, E. Di Valentino, S. Kumar, R. C. Nunes, E. Ozulker, J. A. Vazquez, and A. Yadav, Λ_sCDM cosmology from a type-II minimally modified gravity, Mon. Not. Roy. Astron. Soc. **546**, staf2276 (2025), 2402.07716.
[195] A. Gomez-Valent and J. Solà Peracaula, Phantom Matter: A Challenging Solution to the Cosmological Tensions, Astrophys. J. **975**, 64 (2024), 2404.18845.
[196] R. Calderon *et al.* (DESI), DESI 2024: reconstructing dark energy using crossing statistics with DESI DR1 BAO data, JCAP **10**, 048, 2405.04216.
[197] D. Bousis and L. Perivolaropoulos, Hubble tension tomography: BAO vs SN Ia distance tension, Phys. Rev. D **110**, 103546 (2024), 2405.07039.
[198] H. Wang, Z.-Y. Peng, and Y.-S. Piao, Can recent DESI BAO measurements accommodate a negative cosmological constant?, Phys. Rev. D **111**, L061306 (2025), 2406.03395.
[199] E. Ó. Colgáin, S. Pourojaghi, and M. M. Sheikh-Jabbari, Implications of DES 5YR SNe Dataset for ΛCDM, Eur. Phys. J. C **85**, 286 (2025), 2406.06389.
[200] U. K. Tyagi, S. Haridasu, and S. Basak, Holographic and gravity-thermodynamic approaches in entropic cosmology: Bayesian assessment using late-time data, Phys. Rev. D **110**, 063503 (2024), 2406.07446.
[201] Y. Toda, W. Giarè, E. Özülker, E. Di Valentino, and S. Vagnozzi, Combining pre- and post-recombination new physics to address cosmological tensions: case study with varying electron mass and a sign-switching cosmological constant, Phys. Dark Univ. **46**, 101676 (2024), 2407.01173.
[202] M. A. Sabogal, Ö. Akarsu, A. Bonilla, E. Di Valentino, and R. C. Nunes, Exploring new physics in the late Universe's expansion through non-parametric inference, Eur. Phys. J. C **84**, 703 (2024), 2407.04223.
[203] S. Dwivedi and M. Högås, 2D BAO vs 3D BAO: solving the Hubble tension with alternative cosmological models (2024), 2407.04322.
[204] L. A. Escamilla, E. Özülker, Ö. Akarsu, E. Di Valentino, and J. A. Vázquez, Improved late-time fits with wavelet extensions of ΛCDM, Mon. Not. Roy. Astron. Soc. **544**, 836 (2025), 2408.12516.
[205] L. A. Anchordoqui, I. Antoniadis, D. Bielli, A. Chatrabhuti, and H. Isono, Thin-wall vacuum decay in the presence of a compact dimension meets the H_0 and S_8 tensions, JHEP **07**, 021, 2410.18649.
[206] O. Akarsu, B. Bulduk, A. De Felice, N. Katırcı, and N. M. Uzun, Unexplored regions in teleparallel f(T) gravity: Sign-changing dark energy density, Phys. Rev. D **112**, 083532 (2025), 2410.23068.
[207] A. Gómez-Valent and J. Solà Peracaula, Composite dark energy and the cosmological tensions, Phys. Lett. B **864**, 139391 (2025), 2412.15124.
[208] M. T. Manoharan, Insights on Granda–Oliveros holographic dark energy: possibility of negative dark energy at $z \gtrsim 2$, Eur. Phys. J. C **84**, 552 (2024).
[209] M. S. Souza, A. M. Barcelos, R. C. Nunes, Ö. Akarsu, and S. Kumar, Mapping the Λ_sCDM Scenario to f(T) Modified Gravity: Effects on Structure Growth Rate, Universe **11**, 2 (2025), 2501.18031.
[210] V. A. Pai, S. Nelleri, and T. K. Mathew, Dissipative ΛCDM model with causal sign-switching bulk viscous

pressure, Eur. Phys. J. C **85**, 593 (2025), 2409.10919.
[211] P. Mukherjee, D. Kumar, and A. A. Sen, Quintessential Implications of the presence of AdS in the Dark Energy sector, Phys.Rev.D **113**, 063523 (2026), 2501.18335.
[212] R. E. Keeley, K. N. Abazajian, M. Kaplinghat, and A. Shafieloo, Preference for evolving dark energy from cosmological distance measurements and possible signatures in the growth rate of perturbations, Phys. Rev. D **112**, 043501 (2025), 2502.12667.
[213] Ö. Akarsu, L. Perivolaropoulos, A. Tsikoundoura, A. E. Yükselci, and A. Zhuk, Dynamical dark energy with AdS-to-dS and dS-to-dS transitions: Implications for the H_0 tension (2025), 2502.14667.
[214] J. F. Soriano, S. Wohlberg, and L. A. Anchordoqui, New insights on a sign-switching Λ, Phys. Dark Univ. **48**, 101911 (2025), 2502.19239.
[215] M. A. Sabogal, E. Silva, R. C. Nunes, S. Kumar, and E. Di Valentino, Sign switching in dark sector coupling interactions as a candidate for resolving cosmological tensions, Phys. Rev. D **111**, 043531 (2025), 2501.10323.
[216] P. Mukherjee and A. A. Sen, New expansion rate anomalies at characteristic redshifts geometrically determined using DESI-DR2 BAO and DES-SN5YR observations, Rept. Prog. Phys. **88**, 098401 (2025), 2505.19083.
[217] D. Efstratiou and L. Perivolaropoulos, Metastable cosmological constant and gravitational bubbles: Ultralate-time transitions in modified gravity, Phys. Rev. D **111**, 123546 (2025), 2503.11365.
[218] H. Wang and Y.-S. Piao, Can the universe experience an AdS landscape since matter-radiation equality?, Phys. Rev. D **112**, 083553 (2025), 2506.04306.
[219] M. Bouhmadi-López and B. Ibarra-Uriondo, Cosmographic analysis of sign-switching dark energy, Phys. Rev. D **112**, 063559 (2025), 2506.12139.
[220] D. Tamayo, Thermodynamics of sign-switching dark energy models (2025), 2503.16272.
[221] A. González-Fuentes and A. Gómez-Valent, Reconstruction of dark energy and late-time cosmic expansion using the Weighted Function Regression method, JCAP **12**, 049, 2506.11758.
[222] M. Bouhmadi-López and B. Ibarra-Uriondo, Cosmological perturbations for smooth sign-switching dark energy models, Phys. Dark Univ. **50**, 102129 (2025), 2506.18992.
[223] M. Högås and E. Mörtsell, Bimetric gravity improves the fit to DESI BAO and eases the Hubble tension (2025), 2507.03743.
[224] M. Yadav, A. Dixit, A. Pradhan, and M. S. Barak, Empirical validation: Investigating the ΛsCDM model with new DESI BAO observations, JHEAp **49**, 100453 (2026), 2509.26049.
[225] K. Lehnert, Hitchhiker's Guide to the Swampland: The Cosmologist's Handbook to the string-theoretical Swampland Programme (2025), 2509.02632.
[226] H. S. Tan, Inferring Cosmological Parameters with Evidential Physics-Informed Neural Networks, Universe **11**, 403 (2025), 2509.24327.
[227] D. Pedrotti, L. A. Escamilla, V. Marra, L. Perivolaropoulos, and S. Vagnozzi, BAO miscalibration cannot rescue late-time solutions to the Hubble tension, Phys. Rev. D **113**, 043507 (2026), 2510.01974.
[228] M. Forconi and A. Melchiorri, The impact on non-Gaussianities of the ISW-Lensing correlation in non-standard cosmologies, Phys. Dark Univ. **50**, 102126 (2025).
[229] E. N. Nyergesy, I. G. Márián, A. Trombettoni, and I. Nándori, From negative to positive cosmological constant through decreasing temperature of the Universe: connection with string theory and spacetime foliation results (2025), 2510.02244.
[230] P. Ghafari, M. Najafi, M. Ghodsi Yengejeh, E. Özülker, E. Di Valentino, and J. T. Firouzjaee, A Multi-Probe ISW Study of Dark Energy Models with Negative Energy Density: Galaxy Correlations, Lensing Bispectrum, and Planck ISW-Lensing Likelihood (2025), 2512.07060.
[231] N.-M. Nguyen, D. Huterer, and Y. Wen, Evidence for Suppression of Structure Growth in the Concordance Cosmological Model, Phys. Rev. Lett. **131**, 111001 (2023), 2302.01331.
[232] J. D. Barrow, Sudden future singularities, Class. Quant. Grav. **21**, L79 (2004), gr-qc/0403084.
[233] J. Adamek, D. Daverio, R. Durrer, and M. Kunz, General relativity and cosmic structure formation, Nature Phys. **12**, 346 (2016), 1509.01699.
[234] J. Adamek, D. Daverio, R. Durrer, and M. Kunz, gevolution: a cosmological N-body code based on General Relativity, JCAP **07**, 053, 1604.06065.
[235] D. Blas, J. Lesgourgues, and T. Tram, The Cosmic Linear Anisotropy Solving System (CLASS) II: Approximation schemes, JCAP **07**, 034, 1104.2933.
[236] J. Adamek, R. Durrer, and M. Kunz, Relativistic N-body simulations with massive neutrinos, JCAP **11**, 004, 1707.06938.
[237] J. Brandbyge and S. Hannestad, Grid Based Linear Neutrino Perturbations in Cosmological N-body Simulations, JCAP **05**, 002, 0812.3149.
[238] J. Adamek, J. Brandbyge, C. Fidler, S. Hannestad, C. Rampf, and T. Tram, The effect of early radiation in N-body simulations of cosmic structure formation, Mon. Not. Roy. Astron. Soc. **470**, 303 (2017), 1703.08585.
[239] P. Madau and M. Dickinson, Cosmic Star Formation History, Ann. Rev. Astron. Astrophys. **52**, 415 (2014), 1403.0007.
[240] G. Barro *et al.*, CANDELS: The progenitors of compact quiescent galaxies at z˜2, Astrophys. J. **765**, 104 (2013), 1206.5000.
[241] A. van der Wel *et al.*, 3D-HST+CANDELS: The Evolution of the Galaxy Size-Mass Distribution since $z = 3$, Astrophys. J. **788**, 28 (2014), 1404.2844.
[242] J. Aird *et al.*, The NuSTAR Extragalactic Surveys: First Direct Measurements of the $\gtrsim$ 10 keV X-Ray Luminosity Function for Active Galactic Nuclei at z >0.1, Astrophys. J. **815**, 66 (2015), 1511.04184.
[243] Y. Ueda, M. Akiyama, G. Hasinger, T. Miyaji, and M. G. Watson, Toward the Standard Population Synthesis Model of the X-Ray Background: Evolution of X-Ray Luminosity and Absorption Functions of Active Galactic Nuclei Including Compton-Thick Populations, Astrophys. J. **786**, 104 (2014), 1402.1836.
[244] M. Kilbinger, Cosmology with cosmic shear observations: a review, Rept. Prog. Phys. **78**, 086901 (2015), 1411.0115.
[245] R. Mandelbaum, Weak lensing for precision cosmology, Ann. Rev. Astron. Astrophys. **56**, 393 (2018), 1710.03235.
[246] J. C. Hill and D. N. Spergel, Detection of thermal SZ-CMB lensing cross-correlation in Planck nominal mission data, JCAP **02**, 030, 1312.4525.
[247] E. M. George *et al.*, A measurement of secondary cosmic microwave background anisotropies from the 2500-

square-degree SPT-SZ survey, Astrophys. J. **799**, 177 (2015), 1408.3161.

[248] Ö. Akarsu, M. Eingorn, L. Perivolaropoulos, A. E. Yükselci, and A. Zhuk, Dynamical dark energy with AdS-dS transitions vs. Baryon Acoustic Oscillations at $z = 2.3$-2.4, (2025), 2504.07299.

[249] Ö. Akarsu, E. Di Valentino, J. Vyskocil, E. Yılmaz, A. E. Yükselci, and O. Zhuk, Data: Nonlinear Matter Power Spectrum from relativistic N-body Simulations: Λ_sCDM versus ΛCDM [Data set] 10.14278/rodare.4019 (2025).

[250] A. J. Mead, C. Heymans, L. Lombriser, J. A. Peacock, O. I. Steele, and H. A. Winther, Accurate halo-model matter power spectra with dark energy, massive neutrinos and modified gravitational forces, Mon. Not. Roy. Astron. Soc. **459**, 1468 (2016), 1602.02154.